Am J Physiol Gastrointest Liver Physiol 319: G669–G684, 2020.
First published September 23, 2020; doi:10.1152/ajpgi.00175.2020.

RESEARCH ARTICLE | *Liver and Biliary Tract Physiology/Pathophysiology*

Assessment of the role of FGF15 in mediating the metabolic outcomes of murine vertical sleeve gastrectomy

Andriy Myronovych,[1,3] Jashdeep Bhattacharjee,[4] Rosa-Maria Salazar-Gonzalez,[1,4] Brandon Tan,[1] Sarah Mowery,[1] Danielle Ferguson,[1] Karen K. Ryan,[5] Wujuan Zhang,[2] Xueheng Zhao,[2] Melissa Oehrle,[2] Kenneth D. R. Setchell,[2] Randy J. Seeley,[3] Darleen A. Sandoval,[3] and Rohit Kohli[1,4]

[1]*Department of Pediatrics, Division of Gastroenterology, Hepatology and Nutrition, Cincinnati Children's Hospital Medical Center, Cincinnati, Ohio;* [2]*Department of Pathology and Laboratory Medicine, Cincinnati Children's Hospital Medical Center, Cincinnati, Ohio;* [3]*Department of Surgery, University of Michigan, Ann Arbor, Michigan;* [4]*Division of Gastroenterology, Hepatology and Nutrition, Children's Hospital Los Angeles, Los Angeles, California; and* [5]*Department of Neurobiology, Physiology and Behavior, University of California, Davis, California*

Submitted 13 May 2020; accepted in final form 16 September 2020

Myronovych A, Bhattacharjee J, Salazar-Gonzalez RM, Tan B, Mowery S, Ferguson D, Ryan KK, Zhang W, Zhao X, Oehrle M, Setchell KD, Seeley RJ, Sandoval DA, Kohli R. Assessment of the role of FGF15 in mediating the metabolic outcomes of murine vertical sleeve gastrectomy. *Am J Physiol Gastrointest Liver Physiol* 319: G669–G684, 2020. First published September 23, 2020; doi:10.1152/ajpgi.00175.2020.—Vertical sleeve gastrectomy (VSG) is the best current therapy for remission of obesity and its comorbidities. It is understood to alter the enterohepatic circulation of bile acids in vivo. Fibroblast growth factor 19 (FGF19) in humans and its murine ortholog Fgf15 play a pivotal role in this bile acid-driven enterohepatic signaling. The present study evaluated the metabolic outcomes of VSG in *Fgf15*-deficient (KO) mice. 6- to 8-wk-old male wild-type (WT) and KO mice were fed a high-fat diet (HFD) for 8 wk. At 8th week of diet, both WT and KO mice were randomly distributed to VSG or sham surgery. Postsurgery, mice were observed for 8 wk while fed a HFD and then euthanized to collect tissues for experimental analysis. KO mice lost weight post-VSG, but glucose tolerance in KO mice did not improve post-VSG compared with WT mice. Enteroids derived from WT and KO mice proliferated with bile acid exposure in vitro. Post-VSG, both WT and KO mice had similarly altered bile acid enterohepatic flux; however, *Fgf15* deficient mice post-VSG had increased hepatic accumulation of free and esterified cholesterol, leading to lipotoxicity-related endoplasmic reticulum stress, inflammasome activation, and increased *Fgf21* expression. We conclude that intact Fgf15-mediated enterohepatic bile acid signaling, but not changes in bile acid flux, appear to be important for the metabolic improvements post-murine bariatric surgery. These novel data introduce a potential point of distinction between bile acids acting as ligands compared with their canonical downstream signaling pathways.

NEW & NOTEWORTHY In the absence of an intact fibroblast growth factor 15 (FGF15) signaling pathway, murine vertical sleeve gastrectomy results in weight loss without all its anticipated metabolic benefits. In the absence of an intact FGF15 signaling pathway, vertical sleeve gastrectomy results in increased intestinal bile acid levels and hepatolipotoxicity.

cholesterol metabolism; glucose tolerance; hepatic lipid metabolomics; liver injury; serum bile acid composition

INTRODUCTION

The prevalence of obesity in the world had doubled since the 1980s (11), and with that the incidence of its comorbidities including but not limited to type 2 diabetes and fatty liver disease (NAFLD) have also increased exponentially (33). Diet and lifestyle interventions typically bring about short-lived weight loss, but sustained weight loss is possible primarily through bariatric surgery (23). Today the most popular bariatric procedure is vertical sleeve gastrectomy (VSG) (56). In addition to the weight loss and improvements in glucose and lipid metabolism, VSG results in a host of physiological changes (52). One example of this is that VSG results in an increase in circulating bile acids, and, importantly, signaling through the bile acid-responsive nuclear transcription factor farnesoid X receptor (FXR), is necessary for VSG-associated weight loss and glucose metabolism outcomes (47). However, the role of the bile acid-FXR pathway post-VSG in the context of NAFLD has not been well outlined. In our previous study (40), we reported that, although the downstream target of FXR, small heterodimer partner (SHP), was important for the prevention of hepatic inflammation and injury postsurgery, the body weight loss and the increase in circulating serum bile acid levels were independent of SHP, pointing to the existence of more than one pathway of FXR-driven effects.

Murine fibroblast growth factor 15 (Fgf15) and its human ortholog fibroblast growth factor 19 (FGF19) are both secreted from the distal small intestine (ileum) in response to FXR activation by bile acids (35). Once secreted, Fgf15/19 reaches the liver through the portal blood flow, binds to FGF receptor 4 (FGFR4) and β-Klotho hepatocyte receptor complex, and mediates hepatic signaling that represses lipogenesis and bile acid synthesis in the liver as a part of a negative feedback loop (22). Available data suggest the possibility that Fgf15/19 may be responsible for the reduction of hepatic triglycerides and systemic inflammation after VSG (19), (38). However, increased serum circulating concentrations of both bile acids and Fgf19 have been reported in patients post-bariatric surgery (48). Alteration of bile acid physiology or enterohepatic circulation have both been given attribution to the beneficial metabolic outcomes of VSG (39), (27). This sets up an interesting dichotomy; therefore, the overall function of Fgf15/19 as a signaling molecule in

Correspondence: R. Kohli (rokohli@chla.usc.edu); D. A. Sandoval (darleens@med.umich.edu).

enterohepatic signaling post-bariatric surgery needs to be elucidated. Our present study aimed to understand the role of changes in both bile acid flux and Fgf15 signaling and their role in the hepatic-specific benefits of VSG. We studied the effect of VSG, in the absence of Fgf15, on bile acid- and FXR-mediated enterohepatic signaling and liver outcomes. We found that mice lacking Fgf15 exhibited a worsening NAFLD phenotype after VSG, including an increased accumulation of liver cholesterol, phosphatidylinositol, diacylglycerol, and phosphatidylglycerol, with exaggerated endoplasmic reticulum (ER) stress and inflammasome activation. Therefore, we conclude that the hepatoprotective effects of VSG are dependent on an intact bile acid-FXR-Fgf15 signaling pathway.

MATERIALS AND METHODS

Experimental design. The research objective of this controlled laboratory experiment was to elucidate whether genetically modified Fgf15 knockout (KO) mice would develop the same metabolic improvements after VSG as their wild-type (WT) littermates. This would make it possible to look further into and dissect the complex FXR mechanism, which was shown to be activated after VSG and which is responsible for the majority of its beneficial effects, while trying to target this mechanism at the FXR level, which is a multifunctional transcription factor and is risky due to potential side effects. Fgf15 is one of the downstream targets of FXR. Therefore, the primary end points of the animal study were body weight and glucose, lipid, cholesterol, and bile acid metabolism in the liver and partly in the intestine post-VSG, while intestinal organoids were used to investigate bile acid dynamics and proliferative effect of bile acid-Fgf15 axis.

Animals. Animal studies were approved by the Institutional Animal Care and Use Committees at Cincinnati Children's Hospital Medical Center and the University of Michigan. Fgf15-KO mice were kindly provided by Steven Kliewer, University of Texas Southwestern. Heterozygous Fgf15-KO mice on C57Bl/6 background were used for establishing of the colony utilized in this study. Mice were housed in a temperature-controlled room (22 ± 2°C) on a 12-h:12-h light-dark cycle, and all procedures were performed during the light cycle. Male Fgf15-KO 8 wk old mice and their WT littermates were subjected to a 60% kcal saturated high-fat diet (HFD; Research Diets, New Brunswick, NJ) for 8 wk before surgery. Mice were kept on the same HFD after the surgery. All animals had ad libitum diet and water access and were housed in conventional mouse cages with corn cob bedding and enrichment (cotton nestlet, enviropac).

Surgery and postoperative care. VSG and sham surgeries, and postoperative care were performed as previously described (39). Mice were randomized into VSG [Fgf15-KO (n = 8) and WT (n = 8)] or Sham [Fgf15-KO (n = 5) and WT (n = 6)] surgery groups. Body weight and food intake were monitored on a weekly basis. Blood was collected before surgery and at 14, 28, and 42 days postsurgery for serum sample preparation. At *day 49* postsurgery, all mice were fasted overnight and gavaged with 0.5 mL of liquid diet (Osmolite; Abbott Laboratories, Columbus, OH) 1 h before euthanasia. Serum, hepatic, and intestinal samples were collected at euthanasia. Liver and intestine were collected and snap-frozen in liquid nitrogen or fixed in formalin for histological examination.

In another cohort of mice that was randomized and operated on in the same manner, a carotid artery catheter was implanted and a repeat laparotomy performed 2 wk after VSG [Fgf15-KO (n = 5) and WT (n = 14)] or Sham surgeries [Fgf15-KO (n = 5) and WT (n = 9) mice]. While under isoflurane anesthesia, 0.5 mg of deuterium-labeled taurocholic acid (D_4-TCA; Isosciences, King of Prussia, PA), diluted in 200 μL of saline was injected into the duodenum of each mouse. Blood was collected from the carotid artery before and 30, 60, and 90 min after D_4-TCA administration. Mice were euthanized immediately after the last blood sample collection, and liver samples were harvested for further analysis. Additionally, in a small subset of animals (7 WT Sham and 4 WT VSG), 1.0 mg of D_4-TCA was administered into the duodenum, and their liver samples were collected 90 min thereafter and utilized for hepatic bile acid composition analysis.

Body composition analysis. An Echo MRI Whole Body Composition Analyzer (Echo Medical Systems, Houston, TX) was used to evaluate fat and lean mass of Sham and VSG mice before and 42 days postsurgery.

Oral glucose tolerance test. One week before and 4 wk after surgery, 4-h-fasted mice were administered 20% dextrose by oral gavage (1.5 g/kg). Blood glucose levels were measured before and 15, 30, 45, 60, and 120 min after administration.

Blood glucose and insulin and serum and hepatic triglyceride, cholesterol, alanine aminotransferase, serum FGF21, and bile acid quantification and bile acid composition analyses. Blood glucose was analyzed using a One Touch Glucometer (LifeScan, Milpitas, CA) and plasma insulin levels by ELISA Kit (Crystal Chem, Inc., Downers Grove, IL). Serum (2 μL) and liver (100 mg of tissue homogenized in 1 mL of 20 mM Tris buffer) triglyceride levels (TG) were assessed using a commercially available kit (Triglycerides Reagent Set; Pointe Scientific, Canton, MI). Serum total cholesterol was analyzed using the Cholesterol Reagent Set (Pointe Scientific), while hepatic total and esterified cholesterol using a Cholesterol/Cholesteryl Ester Quantification Kit (Millipore's Calbiochem, Billerica, MA). For alanine aminotransferase (ALT) measurement, kinetic absorbance was read at 340 nm using Discret Pak ALT Reagent Kit (Catachem, Bridgeport, CT). Serum bile acids were evaluated using a Total Bile Acids Assay Kit (Bio-Quant, San Diego, CA) and serum FGF21 by using a Rat/Mouse FGF-21 ELISA Kit (Millipore, Billerica, MA). All kits were used according to the manufacturers' guidelines. Serum and hepatic bile acid composition and quantification, as well as D_4-labeled bile acid quantification, were performed by electrospray ionization liquid chromatography-mass spectrometry (ESI-LC-MS) as previously described (18).

Global lipidomic analysis by ultraperformance liquid chromatography-quadrupole time-of-flight-mass spectrometry. Liver tissue (~15 mg) obtained from Sham and VSG mice was subjected to exhaustive solvent extraction for lipids. Global lipidomics analysis was performed on a Xevo G2-S quadrupole time-of-flight (Q-TOF) mass spectrometer interfaced with an Acquity ultra-high-performance liquid chromatography (UPLC) system (Waters, Milford, MA) operated in electrospray ionization mode as described previously (58). Briefly, an Acquity CSH C_{18} UPLC column was used to chromatographically separate lipid components over 20-min gradient elution. Compounds were ionized with electrospray, and ions were acquired over the mass range 50–1,200 Da with high resolution under both positive and negative modes. Deconvolution, peak alignment, and preliminary normalization were conducted on raw metabolomics data with Progenesis QI (Waters). Each compound ion feature was annotated by elution time with m/z. Raw data were normalized by total compound ion intensity and with a global scalar derived from logarithm ratio of each sample to the reference. Accurate molecular mass was used to search against the Human Metabolome Database (HMDB) (55) and the lipid MAPS database for lipid identification.

qPCR gene expression evaluation. RNA was prepared from snap-frozen liver tissues or washed organoids according to the TRIzol reagent protocol (Molecular Research Center, Cincinnati, OH). A TaqMan Reverse Transcription kit was used to prepare cDNA (Applied Biosystems, Carlsbad, CA). Reactions were completed in an Eppendorf Mastercycler (Eppendorf, Hamburg, Germany). Relative mRNA expression was evaluated with the FAM real-time kinetic PCR on a Mx-3005 Multiplex Quantitative PCR Machine (Stratagene, Agilent Technologies, La Jolla, CA). Ribosomal 18S gene was used as a standard, and the standard curve method was applied to calculate expression.

For all genes of interest, TaqMan primers were utilized (Applied Biosystems, Carlsbad, CA).

BioMark HD system gene expression evaluation. RNA was used to generate cDNA using Reverse Transcription Master Mix (Fluidigm, San Francisco, CA). The cDNA was preamplified for 14 cycles with primers of the DELTAgene Assay in a multiplex PCR reaction using PreAmp Master Mix (Fluidigm). The preamplified PCR products were treated with Exonuclease I (New England Biolabs, Ipswich, MA), diluted fivefold using TE buffer (TEKnova, Hollister, CA) and used as samples in the inlets of primed Dynamic Array 96.96 GE IFC (Fluidigm). A 5 μM concentration of each primer of DELTAgene Assay was added to assay inlets. The real-time PCR data were collected using the Biomark HD, with each sample having four replicates. The fold change of gene expression was calculated using Fluidigm Real-Time PCR Analysis software (Fluidigm).

Histology. Hematoxylin-eosin (H&E)-stained sections were prepared in the Histology Core Services of Cincinnati Children's Hospital Digestive Disease Research Center. Images were taken with an Olympus BX51TF microscope (Olympus Corp., Tokyo, Japan). For apical sodium-dependent bile acid transporter (Asbt) identification in the terminal ileum by immunofluorescence, sections were incubated with anti-Asbt antibody (Santa Cruz Biotechnology, Dallas, TX). Morphometric analysis of ileum cross sections was analyzed by Image-Pro Plus software (Media Cybernetics, Bethesda, MD).

Ileum organoid preparation and utilization. Ileum-derived organoids were prepared as described (36). Briefly, small intestine was extracted from WT and Fgf15 KO male mice and flushed with cold PBS. Ileum was opened longitudinally and cut in 5-mm pieces, which were transferred into 5 mL of cold PBS, washed at 4°C for 5 min, and then processed in epithelial removal buffer for 30 min at 4°C. Remaining intestinal tissue was hand shaken in dissociation buffer for 2 min, visualized, and counted under a light microscope (×5). Crypt suspension was filtered in a 70 μM cell strainer and centrifuged at 150 *g* for 10 min. Crypt fraction containing 200–500 crypts per well was centrifuged at 150 *g* for 10 min at 4°C. The pellet was suspended in 50 μL of Matrigel (Corning Inc., Corning, NY), supplemented with R-spondin 1 (1 g/mL), Noggin (100 ng/mL), and epidermal growth factor (EGF; 50 ng/mL) (all 3 from R&D Systems, Minneapolis, MN). Crypt-Matrigel suspension was cultured in a 24-well plate in a CO_2 incubator (37°C, 5% CO_2) for 20 min to allow complete polymerization of the Matrigel and after that overlaid with 500 μL of basal mini gut medium. Following this, plates were placed back into the incubator. Four- to five-day-old organoids were cultured with 40 μM cholic acid (CA), 400 μM taurocholic acid (TCA), or medium alone (control) overnight. DMEM-F12 at 1:1 was used as a medium (Thermo Fisher Scientific, Waltham, MA), supplemented with penicillin-streptomycin, glutamine, and HEPES. Next morning, proliferation was assessed by fluorescence proliferation detection assay Click-iT Edu Alexa Fluor 594 imaging kit (Thermo Fisher Scientific). E-cadherin primary antibody was used to visualize epithelial cell type, and counterstaining was done with DAPI for nucleus visualization. Organoids were imaged using a Nikon A1 inverted confocal microscope (Nikon Instruments Inc., Melville, NY). Analysis and count of cell proliferation were performed using the Bitplane Imaris program (Bitplane Oxford Instruments, Concord, MA).

Statistical analysis. All values are expressed as means ± SE. Statistical analyses were performed using GraphPad Prism Software (version 7). Statistical significance was evaluated by one- or two-way ANOVA and, where indicated, Student's *t* test to compare two groups. P values < 0.05 were considered to be significant. Serum bile acid composition data were not normally distributed and were therefore expressed as log transformed. For untargeted lipidomics analysis, discovery of lipid features significantly altered between two groups (WT VSG vs. Fgf15-KO VSG) was conducted with univariate analysis. Statistical significance was determined using both fold changes and P values by two-tailed Student's *t* test. All statistical analyses for lipidomics data were conducted with the R language and environment for statistical computing.

RESULTS

Fgf15 deficiency exacerbates glucose intolerance despite loss of body weight post-VSG. Fgf15-deficient mice (KO) fed HFD for 8 wk weighed less than WT (KO: 28.15 ± 1.08 g vs. WT: 32.80 ± 1.19 g; Fig. 1*A*). HFD-fed KO mice had impaired oral glucose tolerance (Fig. 1*B*). Post-VSG, both WT and KO mice lost significant body weight compared with the respective Sham surgery animals despite no difference in food intake among the groups (WT VSG: 17.13 ± 2.45%; KO VSG: 18.03 ± 1.71%; Fig. 1, *C–E*).This was predominantly due to a loss in body fat, as both WT and KO mice had significantly less body fat percentage after VSG compared with the respective Sham surgery mice (WT Sham: 30.59 ± 2.8% vs. WT VSG: 16.34 ± 2.12%; KO Sham: 21.03 ± 3.57% vs. KO VSG: 10.27 ± 1.38%; Fig. 1*F* and Supplemental Figure S1; all supplemental material is available at https://doi.org/10.6084/m9.figshare.12909980). WT VSG mice had improved glucose tolerance compared with the WT Sham surgery mice, but KO mice showed no improvement in glucose tolerance post-VSG (Fig. 1*G*). We also observed lower postprandial blood glucose in both WT and KO VSG mice compared with the respective Sham surgery mice (Supplemental Fig. S2), but plasma insulin concentration decreased only in WT VSG mice (Supplemental Fig. S3). KO VSG mice had a higher insulin-to-glucose ratio compared with WT Sham, WT VSG, and KO Sham (Fig. 1*H*). Finally, we observed that two genes involved in insulin signaling, *Pik3r1* (phosphoinositide 3-kinase regulatory subunit 1) and *Akt3* (RACγ serine/threonine-protein kinase) had higher expression, whereas *Akt1* (RACα serine/threonine protein kinase) and *Akt2* (RACβ serine/threonine-protein kinase) were significantly downregulated in KO VSG compared with WT VSG mice in the liver (Fig. 1*I*). Therefore, these data suggest that *Fgf15* is necessary for the improvement in glucose metabolism following VSG.

Bile acid exposure increases ileal proliferation both in vitro and in vivo. In our previous publication (29), we reported that bariatric surgery increased luminal bile acid content and altered enterohepatic circulation in vivo. Ileal enteroids derived from WT mice incubated with 40 μM cholic acid in vitro had increased proliferation compared with their medium control (Figs. 2, *A* and *B*). We observed increased expression of *Fgf15* in the WT mouse derived ileal enteroids when incubated with bile acids CA and TCA (Fig. 2*C*). The morphometric analysis of ileum cross sections of both WT and KO mice (Fig. 2*D*) revealed that KO mice had both increased villi surface area (Fig. 2*E*) and volume (Fig. 2*F*). Subsequently, Asbt-positive staining was increased in Fgf15-KO mice that had VSG compared with the WT VSG group, suggesting that these mice had increased BA resorption (Fig. 2, *G* and *H*). However, this may have been a result of a compensatory mechanism, because disruption of *Fgf15* signaling in the ileum results in higher bile acid intraluminal content (34). Therefore, we hypothesized that our *Fgf15*-deficient mice also had similarly increased intraluminal bile acid exposure, which in turn induced epithelial proliferation in the ileum of KO mice.

Enterohepatic bile acid circulation in WT and KO mice post-VSG. We studied bile acid enterohepatic circulation directly after VSG in both WT and *Fgf15*-deficient mice. We found that both WT and KO mice have a higher concentration of serum bile acids than their respective Sham surgery mice (WT VSG: 76.40 ± 15.79 μM vs. WT Sham: 40.13 ± 2.62 μM;

KO VSG: 64.61 ± 8.87 μM vs. KO Sham: 29.79 ± 6.43 μM); Fig. 3*A*). Serum bile acid composition analysis by mass spectrometry revealed that WT VSG mice haved a higher abundance of taurine-conjugated and -unconjugated primary bile acids compared with WT Sham mice. In KO VSG mice, we observed a similar overall trend compared with the KO Sham group (Fig. 3*B*). However, the magnitude of the fold change in bile acid abundance (VSG to Sham) was much higher in WT compared with that of KO mice (Supplemental Fig. S4). No difference in total hepatic bile acid content was present between the groups

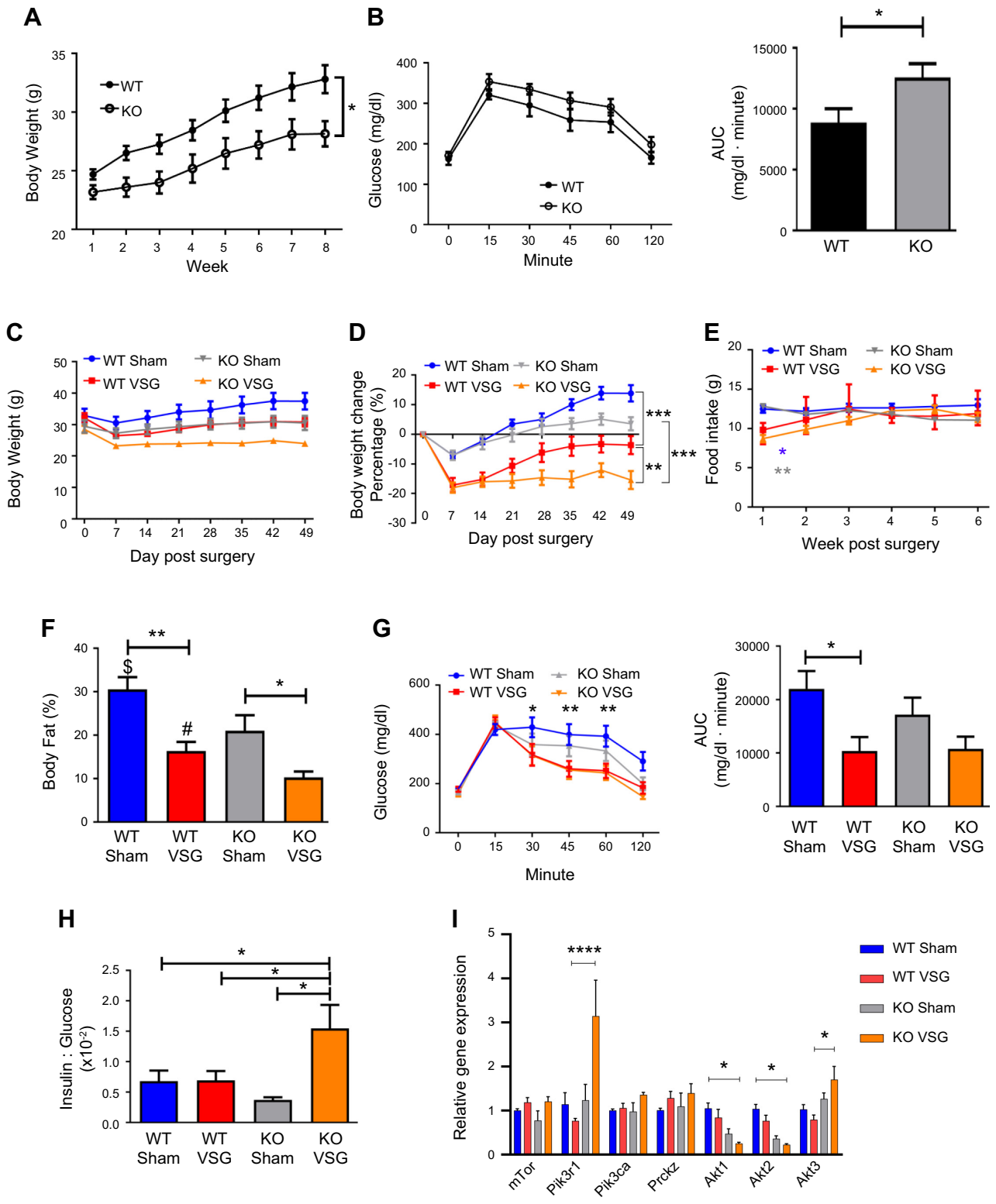

(Fig. 3*C*). However, as revealed by mass spectrometry, several individual bile acids and total unconjugated bile acid levels were significantly higher in WT VSG mice compared with WT Sham mice. This was not observed between KO VSG and KO Sham mice (Fig. 3*D*). KO Sham group exhibited significantly higher levels of total bile acids in the ileum (Fig. 3*E*). Several individual taurine conjugated and unconjugated bile acids, conjugated and total bile acid levels were significantly higher in KO Sham mice compared with KO VSG mice. This was not observed between WT VSG and WT Sham mice (Fig. 3*F*). Hepatic expression of key cholesterol metabolism and bile acid synthesis genes like *Cyp7a1* (cytochrome P-450-7a1) and *Cyp8b1* and bile acid uptake transporters *Ntcp* (Na^+/taurocholate cotransporting polypeptide), *Oatp2* (sodium-independent organic anion-transporting polypeptide 2), and *Oatp4* (sodium-independent organic anion-transporting polypeptide 4) were significantly lower in VSG vs. Sham surgery mice (WT and KO; Fig. 3*G*); however, expression of bile acid efflux transporter *Bsep* (bile salt export pump) was downregulated in WT VSG but upregulated in KO VSG mice compared with their respective control groups (Supplemental Fig. S5). There was a significant decrease in *Cyp27a1* in WT VSG compared with the WT Sham group, and we observed a similar trend in KO VSG vs. KO Sham mice, this did not reach statistical significance. Next, we measured deuterium-labeled taurocholic acid (D_4-TCA) in the systemic circulation after injecting it into the duodenum of mice 2 wk post-VSG or Sham surgery. We observed higher labeled bile acid concentration in the systemic circulation but not in the liver (Supplemental Fig. S6) of mice post VSG compared with Sham-operated mice regardless of genotype (Fig. 3*H*). Thus, we conclude that *Fgf15* is not necessary for the dramatic changes in bile acid enterohepatic circulation after VSG in mice.

Fgf15 deficiency is associated with accumulation of esterified cholesterol and hepatolipotoxicity in mice post-VSG. Hepatic triglyceride content decreased in both WT and KO mice post VSG compared with their respective Sham surgery mice (WT Sham: 8.24 ± 1.0 mg vs. WT VSG: 2.69 ± 0.37 mg; KO Sham: 6.95 ± 1.64 mg vs. KO VSG: 2.42 ± 0.36 mg) (Fig. 4*A*). While surgery had no impact on liver weight relative to body weight in WT mice, the KO VSG mice had significantly higher liver weight to body weight ratio compared with KO Sham (Fig. 4*B*). Both VSG groups had lower fasting serum cholesterol levels compared with their respective Sham groups early postsurgery (Supplemental Fig. S6). However, we observed that both WT and KO VSG mice had increased concentrations of hepatic free cholesterol compared with their respective Sham controls (Fig. 4*C*), but only KO VSG mice exhibited an increase in esterified cholesterol (Fig. 4*D*). Hepatic expression of 3-hydroxy-3-methyl-glutaryl-CoA reductase (*HMG-CoA*), the rate-limiting enzyme for cholesterol synthesis, was decreased post-VSG in WT but not in KO VSG mice livers. KO VSG mice also had lower hepatic expression levels of cholesterol efflux pump-ATP-binding cassette, subfamily G (WHITE), member 5 (sterolin 1, *Abcg5*) and ATP-binding cassette, subfamily G (WHITE), member 8 (sterolin 2, *Abcg8*) compared with WT Sham, WT VSG, and KO Sham mice (Fig. 4*E*). Finally, fatty acid oxidation and fatty acid metabolism like carnitine palmitoyltransferase-1A (*Cpt1a*), *CD36*, and stearoyl-CoA desaturase (*Scd1*) were decreased post-VSG in WT but not in KO VSG mouse livers (Fig. 4*F*). We further observed that genes involved in fatty acid synthesis: *Acc1* (acetyl-CoA carboxylase-1), *Acc2*, and *Fasn* (fatty acid synthase), and in fat deposition, *PPARγ* (peroxisome proliferator-activated receptor-γ) had higher expression in KO VSG compared with WT VSG and KO Sham mice. In the WT VSG group, hepatic expression of *Acc2*, *Fasn*, and *PPARγ* decreased compared with WT Sham mice (Fig. 4*G*). Further from our data on global lipidomics in liver, we observed higher accumulation of diacylglycerol (DAG), phosphatidylinositol (PI), and phosphatidylglycerol (PG) lipid classes in KO VSG compared with WT VSG mice (Fig. 4, *H–J*). Thus, we conclude that *Fgf15* deficiency induces accumulation of esterified cholesterol and lipids in the liver post-VSG.

Fgf15 deficiency results in increased hepatic inflammation via an ER stress mechanism post-VSG. Histological analysis of the liver revealed that VSG aggravates inflammation in KO but not in WT mice (Fig. 5*A*). The NAFLD activity score (NAS) was significantly higher in KO VSG vs. WT VSG, KO Sham, and WT Sham mice (Fig. 5*B*). We observed no significant difference in this inflammation score between WT VSG and WT Sham mice. Plasma ALT levels were significantly decreased in WT VSG compared with WT Sham mice, but there was no difference in plasma ALT levels in KO Sham vs. KO VSG mice (Fig. 5*C*). We further observed that post-VSG mice had higher expression of hepatic inflammatory cytokine genes like interferon-γ (*IFNγ*), interleukin-17 (*Il17*), tumor necrosis factor-α (*TNFα*), and inflammasome

Fig. 1. Fibroblast growth factor 15 (*Fgf15*) deficiency exacerbates glucose intolerance despite loss of body weight post-vertical sleeve gastrectomy (VSG). *A*: presurgery body weight dynamics in wild-type (WT) and knockout (KO) mice. Both groups gained weight on high-fat diet (HFD); however, KO mice were much lighter than WT mice; *n*: WT = 12, KO = 12. $^*P < 0.05$, one-way ANOVA. *B*: oral glucose tolerance test presurgery and area under the curve (AUC). WT mice before surgery had lower glucose excursions compared with their KO littermates; *n*: WT = 9, KO = 9. $^*P < 0.05$, *t* test. *C*: postsurgery body weight in WT and KO mice. Both VSG groups lost more weight than their respective Sham groups. However, because of KO VSG group's postsurgery body weight plateau, it became significantly lighter compared with WT VSG group; *n*: WT Sham = 6, WT VSG = 6, KO Sham = 5, KO VSG = 7. *D*: postsurgery body weight percentage loss in WT and KO mice. KO VSG mice had the maximum body weight loss percentage postsurgery; *n*: WT Sham = 6, WT VSG = 6, KO Sham = 5, KO VSG = 7. $^{**}P < 0.01$, $^{***}P < 0.0001$, two-way ANOVA. *E*: weekly average food intake. Both VSG groups consumed much less food during the first week after surgery compared with both Sham groups. No difference in food consumption was observed between VSG groups; *n*: WT Sham = 6, WT VSG = 6, KO Sham = 5, KO VSG = 7. $^*P < 0.05$, WT Sham vs. WT VSG, $^{***}P < 0.0001$, KO Sham vs. KO VSG, two-way ANOVA. *F*: body fat content postsurgery. Fat mass was greater in Sham groups compared with their respective VSG groups. Furthermore, fat ratio was much lower in KO VSG compared with WT VSG mice; *n*: WT Sham = 6, WT VSG = 6, KO Sham = 5, KO VSG = 7. $^*P < 0.05$, $^{**}P < 0.01$, $\$P < 0.05$ WT Sham vs. KO Sham, $\#P < 0.05$ WT VSG vs. KO VSG, one-way ANOVA, *t* test). *G*: oral glucose tolerance test 28 days postsurgery and area under the curve. Blood glucose levels were lower in both VSG groups compared with their Sham groups; *n*: WT Sham = 6, WT VSG = 6, KO Sham = 5, KO VSG = 7. $^*P < 0.05$, $^{***}P < 0.01$, one-way ANOVA. *H*: insulin/glucose ratio 14 days postsurgery. Insulin/glucose ratio was decreased in all groups except KO VSG; *n*: WT Sham = 6, WT VSG = 6, KO Sham = 5, KO VSG = 7. $^*P < 0.05$, one-way ANOVA. *I*: hepatic insulin signaling gene expression at *day 49* postsurgery. mRNA levels of genes coding for insulin signaling were measured by Biomark HD System high-throughput PCR and expressed in relative expression units. *Pik3r1* and *Akt3* genes were significantly overexpressed, whereas *Akt1* and *Akt2* were downregulated in KO VSG compared with WT VSG mice; *n*: WT Sham = 4, WT VSG = 5, KO Sham = 4, KO VSG = 6. $^*P < 0.05$, $^{**}P < 0.01$, $^{****}P < 0.0001$, one-way ANOVA.

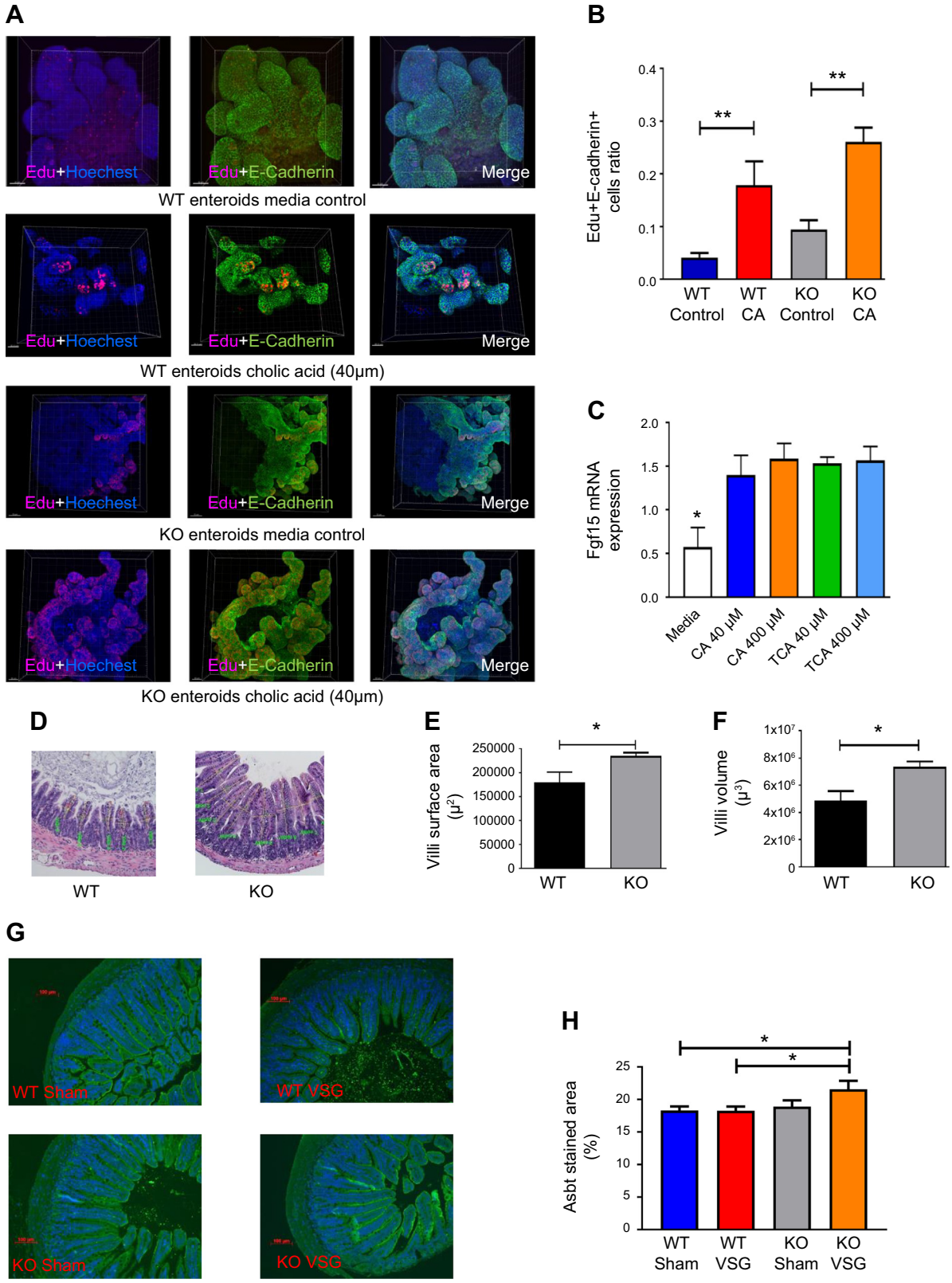

marker (*Nlrp3*) in both WT and KO groups, but this increase was even higher in KO VSG vs. WT VSG mice (Fig. 5*D*). Finally, we observed an increased hepatic expression of genes involved in ER stress in KO VSG compared with WT VSG and KO Sham groups. Hepatic expression of CCAAT enhancer-binding protein homologous protein (*Chop*), a downstream target of protein kinase RNA-like endoplasmic reticulum kinase (*Perk*), mediated ER stress and was significantly higher in KO Sham and KO VSG compared with their respective WT counterparts. Interestingly, post-VSG, we observed a significant decrease in *CHOP* expression in WT VSG compared with WT Sham mice, a surgery effect that was not detected in KO mice (Fig. 5*E*). ER stress is known to induce the hepatic expression of fibroblast growth factor 21 (*Fgf21*) (50). Consistent with this, the KO mice had significantly elevated *Fgf21* expression post-VSG, whereas in WT VSG mice there was a significant decrease in hepatic *Fgf21* expression (Fig. 5*F*). Genes that stimulate Ffg21 production in the liver, *PPARα* and *PGC-1α* (PPARγ coactivator 1α), were assessed. *PPARα* hepatic expression was much lower in WT VSG mice compared with KO VSG mice, whereas expression of *PGC-1α* was significantly higher in KO VSG mice compared with other groups (Fig. 5*G*). Like hepatic expression, we observed a significant decrease in plasma Fgf21 concentration after VSG in WT but a significant increase of plasma Fgf21 levels in KO mice (Fig. 5*H*). Interestingly, many of the *Fgf21*-dependent genes that take part in cholesterol metabolism were overexpressed in KO VSG but downregulated in WT VSG mice (Supplemental Fig. S8). Thus, our data suggest that Fgf15 plays a hepatoprotective role in alleviating ER stress-mediated hepatic inflammation post-VSG.

DISCUSSION

Here, we report that Fgf15 deficiency results in an increased ileal absorptive area potentially attributed to the lack of Fgf15 enterohepatic feedback leading to increased hepatic bile acid production and higher luminal bile acid content and intestinal proliferation observed in KO mice. It has been previously reported that reduced expression of Fgf15 in mice leads to increased gastrointestinal motility and increased luminal bile acid content similar to a human bile acid diarrhea phenotype (34). Once mice were made obese on an HFD and subsequently subjected to weight loss surgery, we observed the Fgf15-deficient animals to have increased hepatic accumulation of free and esterified cholesterol alongside an upregulation of hepatic sterol biosynthesis genes and downregulation of cholesterol efflux pathways. This accumulation of cholesterol was further associated with accumulation of DAGs and PI and increased hepatic ER stress that in turn led to increased hepatic inflammation in KO mice post-VSG (Fig. 6). This is consistent with recent observation of hepatic inflammatory cell infiltrations in mice that had reduced FXR and increased oxidative stress (41). Furthermore, we observed that KO mice had worse glucose intolerance post-VSG despite having less body weight gain compared with WT. Interestingly, bile acid physiology changes observed post-VSG, including bile acid flux, were similar between the WT and KO mice. Thus, in our study, we demonstrated that Fgf15 deficiency has a profound effect on the hepatic metabolic and inflammatory end points downstream of enterohepatic bile acid signaling but no such demonstrable effect on bile acid physiology. This is a potentially critical point in our understanding of the disconnect between bile acid enterohepatic cycling and its impact on hepatic lipogenesis and inflammation.

Bile acid metabolism was not impacted by the Fgf15 deficiency in a murine VSG model, which points to the fact that this molecule is not crucial for its regulation. In our previous study, we discovered that small heterodimer partner (SHP) is not essential for bile acid metabolism regulation either (40). Hepatic FXR acts through SHP and liver-related homolog-1 (LRH-1) to suppress bile acid synthesis through inhibition of Cyp7a1 and Cyp8b1 (8). Thus, neither intestinal nor hepatic FXR pathways were important for bile acid synthesis regulation after VSG. There could be some degree of overcompensation between Fgf15 and SHP, as stimulation in a postprandial state by intestinal FXR, FGF15/19 synergizes with SHP to downregulate bile acid synthesis (22). Alternatively, bile acid metabolism could be affected by another FXR agonist molecule, as shown in a recent study where suppression of bile acid synthesis was induced by FXR agonist Px-102, in a FGF19-independent manner, since it was observed before the onset of increased circulating levels of FGF19 (1).

The evidence of the impact of FXR on obesity, glucose metabolism, and NAFLD may seem contradictory. One study (44) indicated that FXR deficiency attenuated weight gain, improved glucose metabolism by increased peripheral disposal, and alleviated fatty liver disease. However, this was only detected in genetically obese *ob*/*ob* mice. Those authors also observed that total, but not liver-specific, FXR deficiency protects from diet-induced obesity and insulin resistance. Nevertheless, the same group reported that FXR-specific synthetic agonist GW4064 enhanced insulin signaling and insulin-stimulated glucose uptake. Even *ob*/*ob* mice treated with GW4064 improved their

Fig. 2. Bile acid exposure increases ileal proliferation both in vitro and in vivo. *A*: 5-ethynyl-2′-deoxyuridine (EdU) staining of wild-type (WT)- and knockout (KO)-derived cholic acid (CA)-treated intestinal organoids. Ileum-derived ileal organoids actively proliferate when treated with 40 μM CA. E-cadherin (green), EdU proliferation (red), DAPI nucleus (blue); ×20 magnification. *B*: Edu/E-cadherin ratio of CA-treated intestinal organoids. Cell proliferation marker EdU incorporation was significantly increased in both WT- and KO-derived intestinal organoids after 40 μM CA treatment compared with organoids cultured in medium without CA addition; *n*: WT control = 11, WT CA = 11. $^{**}P < 0.01$, *t* test). *C*: fibroblast growth factor 15 (Fgf15) expression in intestinal organoids after bile acid addition. Treatment of WT-derived intestinal organoids with 40 μM and 400 μM concentrations of CA and taurocholic acid (TCA) resulted in increased expression of Fgf15 gene; *n*: medium = 12, CA 40 μM = 12, CA 400 μM = 12, TCA 40 μM = 12, TCA 400 μM = 9. $^{*}P < 0.05$, one-way ANOVA. *D*: hematoxylin-eosin-stained terminal ileum sections of WT and KO mice. Representative ×20 magnified terminal ileum sections. Drastic differences were not observed during morphological examination of the sections. *E*: villi surface area of WT and KO mice. Villi surface area of KO mice was significantly larger compared with WT mice; *n*: WT = 5, KO = 5. $^{*}P < 0.05$, *t* test). *F*: villi volume of WT and KO mice. Villi volume of KO mice was significantly higher compared with WT mice; *n*: WT = 5, KO = 5. $^{*}P < 0.05$, *t* test. *G*: representative ×20 magnified terminal ileum sections stained with apical sodium-dependent bile acid transporter (Asbt) antibody (green). *H*: Asbt surface area staining quantification in the ileum of WT and KO mice. Quantification is expressed as a ratio of Asbt antibody-stained area to total area. Stained area was larger in KO vertical sleeve gastrectomy (VSG) mice compared with mice of WT groups; *n*: WT Sham = 10, WT VSG = 14, KO Sham = 7, KO VSG = 13. $^{*}P < 0.05$, *t* test.

insulin resistance (5). Another study described improvement of NAFLD after intestinal FXR inhibition, where the methods of intestinal microbiota modification were used to increase bile acid metabolites that suppress FXR (24). We utilized a murine model of VSG in our study, and our data indicate that the bile acid-FXR-Fgf15 axis provides beneficial metabolic outcomes after this complex procedure. This all points toward the extreme complexity of FXR as a multifunctional, multilocational nuclear factor; thus, interpretation of experimental results should be done in a more nuanced fashion for each study.

It has been previously reported that Fgf15-deficient mice had impaired liver regeneration after partial hepatectomy (30). Fgf15-deficient mice were shown to be glucose intolerant and had reduced postprandial hepatic glycogen storage (28). Fgf15 has also been shown to play a pivotal role in maintaining hepatic lipid storage and metabolism. Our data support these findings, as we report that KO mice post-VSG had higher expression of genes like *Fasn* and *PPARγ* involved in lipid synthesis, and an accumulation of esterified cholesterol in liver. Hepatic accumulation of esterified cholesterol has previously been linked to a range of

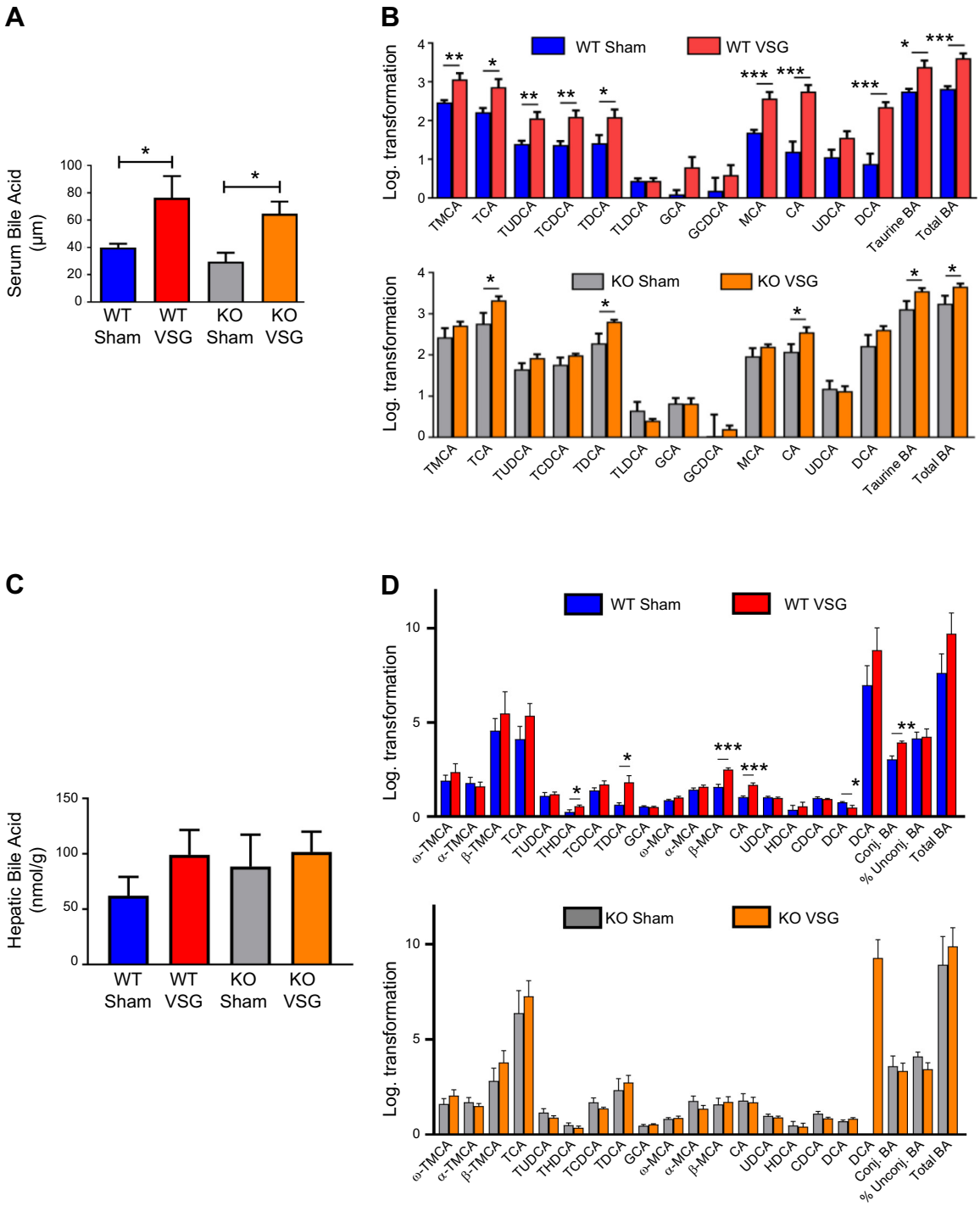

liver diseases from fatty liver disease to obstructive jaundice (53). Thus, our data suggest that, in the absence of an intact Fgf15 pathway, mice post-VSG have a harmful hepatic lipid accumulation.

Fgf15-deficient mice developed insulin resistance after VSG, as they showed increased insulin levels postsurgery despite significant body weight loss. It has been shown that mice lacking Akt2 exhibit insulin resistance and a diabetes mellitus-like syndrome (10), whereas activation of Akt3 may be viewed as a compensatory reaction for the Akt2 deficiency (21). Another study concluded that *Pik3r1* deletion markedly improves insulin sensitivity (54). In our study, Fgf15-KO mice exhibited significant downregulation of Akt2 and overexpression of Pik3r1 and Akt3 in their livers after VSG. Insulin resistance could also be potentially explained by impaired DAG metabolism in these mice. Phosphatidylinositol is utilized for the DAG synthesis, whereas DAGs may be converted back to phosphatidylinositol (16). Conversely, DAG is a substrate for phosphatidylglycerol biosynthesis (6). It is known from basic and clinical studies that activation of protein kinase Cε (PKCε) by DAGs triggers hepatic insulin resistance (49). Moreover, DAG content and PKCε activation in the liver are the strongest predictors of hepatic insulin resistance in obese individuals (31). DAGs, in turn, are a substrate for triglyceride synthesis in the liver by the glycerol 3-phosphate pathway (45). Kupffer cell-driven hepatic inflammation is believed to be the consequence of insulin resistance (14). In addition to that, cholesterol-induced activation of macrophages is a prominent component of the inflammation (57). In our study, hepatic content of phosphatidylinositol, phosphatidylglycerol, and DAG was increased in Fgf15-deficient mice after

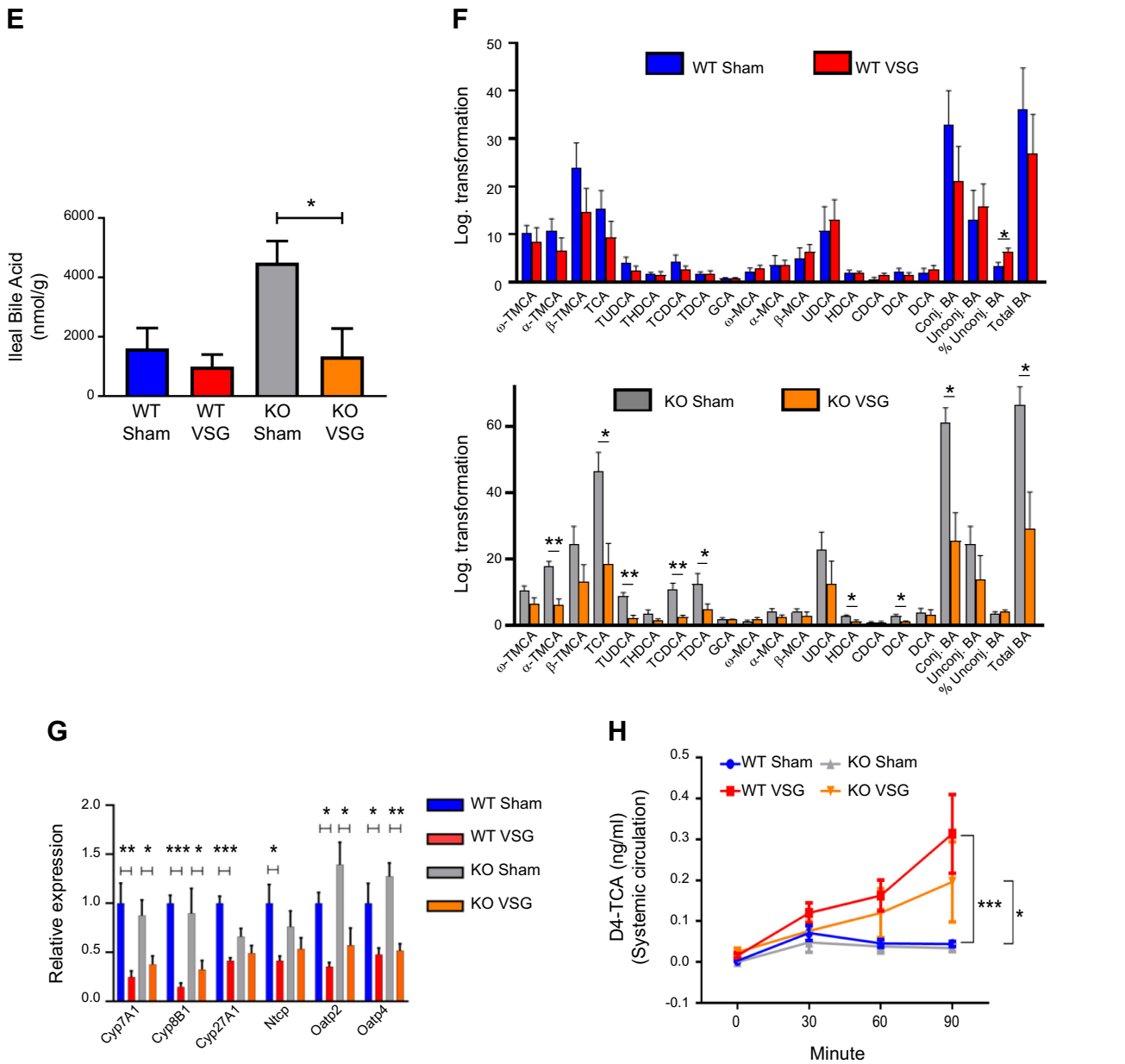

Fig. 3. —*Continued*

VSG. However, hepatic triglycerides were similarly improved in both VSG groups. These data suggest that the pathway to convert DAGs to triglycerides is impaired in mice that lack Fgf15 after VSG.

Our data show the importance of Fgf15 for glucose regulation post-VSG, as KO mice did not show glucose tolerance improvement after surgery according to an oral glucose tolerance test, which was performed in mice after fasting. However, those mice still had significantly lower postprandial glucose levels compared with the KO Sham group, pointing to the activation of another glucose regulation mechanism. Based on our and others' published data, the importance of Fgf15 for glucose homeostasis after VSG should be interpreted with caution. It was shown that Fgf15, introduced by adeno-associated virus-mediated gene delivery, failed to correct hyperglycemia and HbA_{1c} levels and did not improve β-cell mass in diabetic *db*/*db* mice despite its high circulating levels, contrary to its human ortholog FGF19 (59). The impact of Fgf15 and FGF19 on bile acid metabolism was comparable in this model. Another study clearly demonstrated receptor- and species-specific differential activity of Fgf15 and FGF19. While recombinant human FGF19 was able to bind with FGFR1c and FGFR4 in complex with both human and mouse β-Klotho, recombinant murine Fgf15 bound the FGFRs only when combined with mouse β-Klotho. Thus, FGF19 increased glucose uptake in mouse adipocytes, whereas Fgf15 did not. The lack of the effect of Fgf15 on glucose uptake was associated with its inability to signal through the FGFR1c/mouse β-Klotho complex (20). Despite their being commonly referred to as FGF15/19, these results point toward physiological differences between murine Fgf15 and human FGF19, which may not be surprising, taking into account that the amino acid identity between Fgf15 and FGF19 is only ∼50% (43). Considering these differences described in the murine models, and the fact that potentially only FGF19 may be administered in clinical settings, we summarize that our data provide only preliminary insight and that subsequent clinical studies are needed to evaluate the effect of FGF19 on glucose metabolism after VSG.

Interestingly, before surgery, Fgf15-deficient mice were in fact protected from hepatic steatosis, inflammation, and fibrosis when fed a HFD (51). Similarly, in our hands the KO Sham mice had low expression of inflammatory genes in liver, whereas post-VSG the KO mice had an aggravated hepatic inflammatory response compared with the WT VSG group. This trend was further replicated in the observed Fgf21 response, where the concentration of circulating Fgf21 has been reported to be increased during obesity-related hepatic ER stress (25). Fgf21 in mice was shown to increase energy expenditure in the liver and reduced hepatic triglyceride levels (4). This may be explained by the Ire1α-Xbp1 and Perk signaling pathways-mediated increase of Fgf21 expression, which is able to reduce hepatic ER stress-related lipogenesis (25, 26). Fgf21 was also reported to have a beneficial effect on improving glucose metabolism and decreasing cholesterol levels (13). However, under the condition of free fatty acid overload, the action of Fgf21 on lipid metabolism becomes impaired and it may stimulate PPARγ and other lipid synthesis genes that are downstream of this transcription factor (3). In our study, we observed an increased level of circulating Fgf21 and Ire1α-Xbp1, Perk, and PPARγ gene overexpression in KO mice post-VSG compared with KO Sham mice. Fgf21 hepatic expression is stimulated by PPARα (35), while increased Fgf21 levels are associated with PGC-1α overexpression (32). This is in line with our observation of increased Fgf21 serum levels in KO VSG and decreased levels of this factor in WT VSG mice, as PGC-1α gene expression was much higher in the Fgf15-KO VSG group whereas WT VSG mice exhibited lower expression of PPARα in the liver. Despite the Fgf21 elevation, Fgf15-deficient mice did not improve significantly their glucose metabolism after VSG but exhibited overexpression of the cholesterol genes and accumulation of the cholesterol in the liver. Fgf21 elevation in the knockout mice post-VSG appeared to be a putative adaptive response to ER stress to prevent liver damage; however, it was not sufficient to provide hepatic protection and avert accumulation of cholesterol, DAGs, and its intermediates in the liver. Therefore, our data support the conclusion that Fgf15-dependent signaling may play a unique role in the manifestation of metabolic benefits that follows post-VSG,

Fig. 3. Enterohepatic bile acid (BA) circulation in wild-type (WT) and knockout (KO) mice after vertical sleeve gastrectomy (VSG). *A*: total serum bile acid levels at *day 49* postsurgery. Serum bile acid levels were higher in both VSG groups compared with Sham groups 49 days postsurgery; *n*: WT Sham = 6, WT VSG = 6, KO Sham = 5, KO VSG = 7. $*P < 0.05$, one-way ANOVA, *t* test. *B*: serum bile acid composition analysis at *day 49* postsurgery. Most individual bile acids were elevated in serum of WT mice after VSG, whereas both VSG groups had increased serum levels of combined taurine-conjugated bile acids and total bile acids compared with their Sham groups. The following bile acids are indicated: tauromuricholate (TMCA), taurocholate (TCA), tauroursodeoxycholate (TUDCA), taurochenodeoxycholate (TCDCA), taurodeoxycholate (TDCA), taurolithocholate (TLCA), glycocholate (GCA), glycochenodeoxycholate (GCDCA), muricholic acid (MCA), cholic acid (CA), ursodeoxycholate (UDCA), and deoxycholate (DCA); *n*: WT Sham = 6, WT VSG = 5, KO Sham = 5, KO VSG = 6. $*P < 0.05$, $**P < 0.01$, $***P < 0.0001$, *t* test). *C*: total hepatic bile acid levels at *day 49* postsurgery. Hepatic bile acid levels were not significantly different between the groups; *n*: WT Sham = 5, WT VSG = 5, KO Sham = 5, KO VSG = 5. *D*: hepatic bile acid composition analysis at *day 49* postsurgery. Levels of THDCA, TDCA, β-MCA, CA, and total unconjugated bile acids were elevated in liver of WT mice after VSG compared with WT Sham group. No significant difference was observed between KO Sham and VSG groups. The following bile acids are indicated: ω-TMCA, α-TMCA, β-TMCA, TCA, TUDCA, THDCA, TCDCA, TDCA, GCA, ω-MCA, α-MCA, β-MCA, CA, UDCA, HDCA, HDCA, DCA; *n*: WT Sham = 5, WT VSG = 5, KO Sham = 5, KO VSG = 5. $*P < 0.05$, $**P < 0.01$, $***P < 0.0001$, *t* test. *E*: total ileal bile acid levels at *day 49* postsurgery. Ileal bile acid levels were higher in KO Sham compared with KO VSG group 49 days postsurgery; *n*: WT Sham = 5, WT VSG = 5, KO Sham = 5, KO VSG = 5. $*P < 0.05$, one-way ANOVA. *F*: ileal bile acid composition analysis at *day 49* postsurgery. Levels of α-TMCA, TCA, TUDCA, TCDCA, TDCA, UDCA, CDCA, and conjugated and total bile acids were elevated in the ileum of KO Sham compared with KO VSG mice. Percent unconjugated bile acids relative to total bile acids was higher in WT VSG compared with WT Sham group. The following bile acids are indicated: ω-TMCA, α-TMCA, β-TMCA, TCA, TUDCA, THDCA, TCDCA, TDCA, GCA, ω-MCA, α-MCA, β-MCA, CA, UDCA, HDCA, HDCA, DCA); *n*: WT Sham = 5, WT VSG = 5, KO Sham = 5, KO VSG = 5. $*P < 0.05$, $**P < 0.01$, *t* test. *G*: hepatic bile acid synthesis and uptake gene expression at *day 49* postsurgery. mRNA levels of genes coding for bile acid production [*Cyp7a1* (cytochrome *P*-450-7a1), *Cyp8b1*, and *Cyp27a1*], bile acid uptake [*Ntcp* (Na^+-taurocholate-cotransporting polypeptide), *Oatp2* (organic ion transporting polypeptide 2), and *Oatp4*) were measured by RT-PCR and expressed in relative expression units. These genes were similarly suppressed in both VSG relative to Sham groups; *n*: WT Sham = 4, WT VSG = 5, KO Sham = 4, KO VSG = 6. $*P < 0.05$, $**P < 0.01$, $***P < 0.0001$, one-way ANOVA, *t* test. *H*: serum deuterium-taurocholic acid (D_4-TCA) concentration after duodenal administration. D_4-TCA serum levels were assessed before and at 30, 60, and 90 min after injection in WT and KO mice after VSG and Sham surgery. D_4-TCA levels were much higher at all time-points in both VSG groups; *n*: WT Sham = 9, WT VSG = 12, KO Sham = 5, KO VSG = 5. $*P < 0.05$, $***P < 0.0001$, two-way ANOVA.

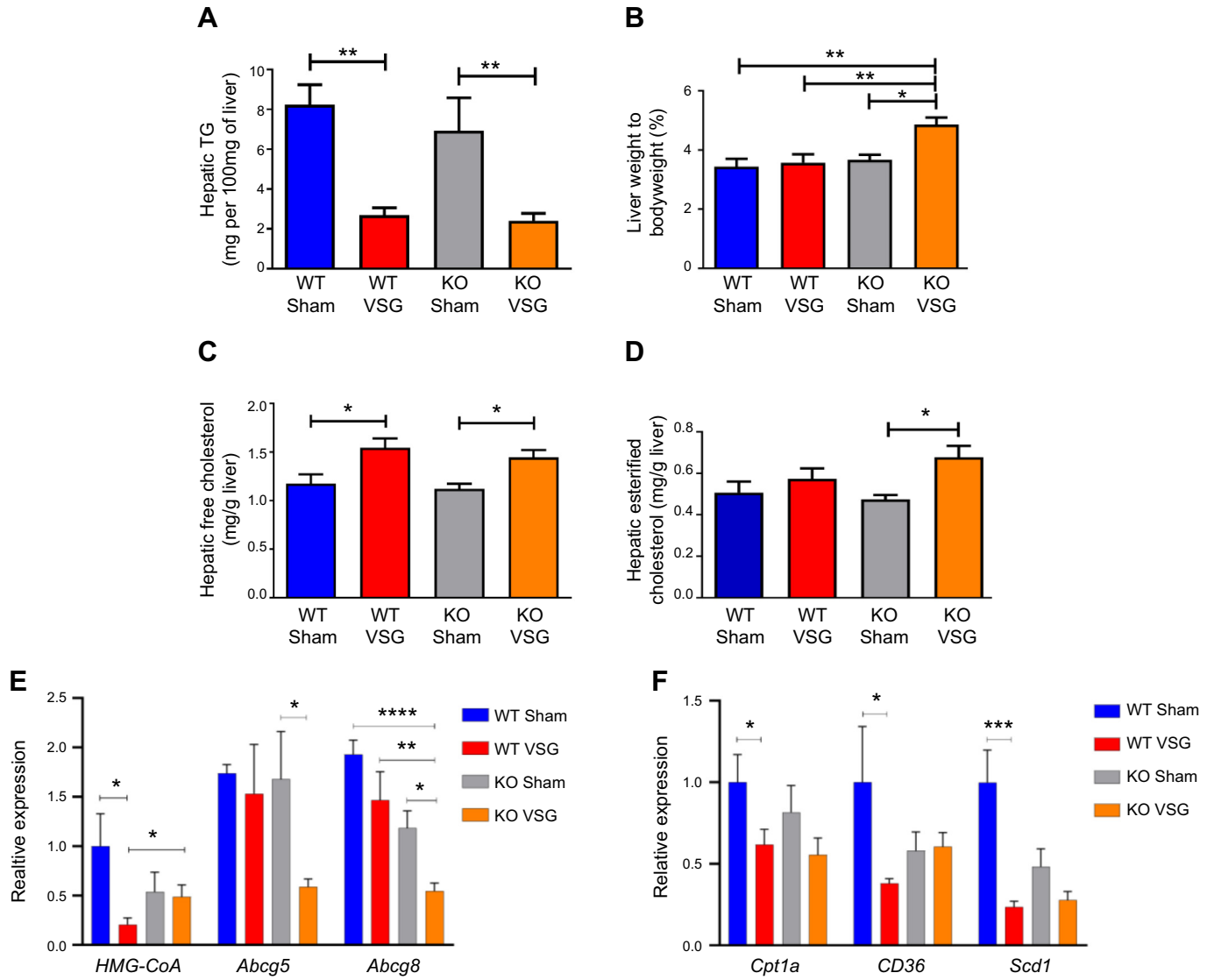

Fig. 4. Fibroblast growth factor 15 (*Fgf15*) deficiency is associated with accumulation of esterified cholesterol and lipotoxicity in mice post-vertical sleeve gastrectomy (VSG). *A*: hepatic triglyceride (TG) content 49 days postsurgery. Liver triglyceride levels were much lower in both VSG groups compared with their respective Sham controls; *n*: wild-type (WT) Sham = 6, WT VSG = 6, knockout (KO) Sham = 5, KO VSG = 7. $^{**}P < 0.01$, one-way ANOVA. *B*: liver weight/body weight ratio 49 days postsurgery. Liver weight/body weight ratio was greater in KO VSG mice compared with all other groups; *n*: WT Sham = 6, WT VSG = 6, KO Sham = 5, KO VSG = 7. $^{*}P < 0.05$, $^{**}P < 0.01$, one-way ANOVA. *C*: hepatic free cholesterol content 49 days postsurgery. Liver free cholesterol levels were elevated in both VSG groups; *n*: WT Sham = 6, WT VSG = 6, KO Sham = 5, KO VSG = 7. $^{*}P < 0.05$, one-way ANOVA. *D*: hepatic esterified cholesterol content 49 days postsurgery. Liver esterified cholesterol levels were elevated in KO VSG group; *n*: WT Sham = 6, WT VSG = 6, KO Sham = 5, KO VSG = 7. $^{*}P < 0.05$, one-way ANOVA, *t* test. *E*: *Hmg-CoA reductase* (3-hydroxy-3-methyl-glutaryl-CoA reductase), *Abcg5*, and *Abcg8* gene expression at *day 49* postsurgery. mRNA levels of the genes coding for the cholesterol synthesis (*Hmg-CoA reductase*), cholesterol efflux pump ATP-binding cassette, subfamily G (WHITE), member 5 (sterolin 1, *Abcg5*), cholesterol efflux pump ATP-binding cassette, subfamily G (WHITE), member 8 (sterolin 2, *Abcg8*) were measured by RT-PCR and expressed in relative expression units. Cholesterol synthesis rate-limiting gene was not downregulated in KO VSG group. Cholesterol export genes were suppressed in KO VSG group; *n*: WT Sham = 4, WT VSG = 4, KO Sham = 4, KO VSG = 6. $^{*}P < 0.05$, $^{**}P < 0.01$, $^{****}P < 0.0001$, one-way ANOVA, *t* test). *F*: *Cpt1a*, *CD36*, and *Scd1* gene expression at *day 49* postsurgery. mRNA levels of the genes coding lipid transport carnitine palmitoyltransferase-1A (*Cpt1a*), lipid synthesis (*CD36*), and lipid synthesis stearoyl-CoA desaturase (*Scd1*) were measured by RT-PCR and expressed in relative expression units. These genes were mostly suppressed in WT VSG group (only trend in KO VSG) relative to Sham group; *n*: WT Sham = 4, WT VSG = 5, KO Sham = 4, KO VSG = 6. $^{*}P < 0.05$, $^{***}P < 0.0001$, one-way ANOVA, *t* test. *G*: hepatic fatty acid oxidation gene expression at *day 49* postsurgery. mRNA levels of genes coding for fatty acid oxidation were measured by Biomark HD System high-throughput PCR and expressed in relative expression units. *Acc1* (acetyl-CoA carboxylase-1), *Acc2*, and *Fasn* (fatty acid synthase) genes were significantly overexpressed only in KO VSG mice; *n*: WT Sham = 4, WT VSG = 5, KO Sham = 4, KO VSG = 6; $^{*}P < 0.05$, $^{**}P < 0.01$, $^{****}P < 0.0001$, one-way ANOVA, *t* test; *n*: WT Sham = 6, WT VSG = 6, KO Sham = 5, KO VSG = 7; $^{*}P < 0.05$, $^{**}P < 0.01$, $^{****}P < 0.0001$, one-way ANOVA. *H*: heat map of significantly changed lipid compounds obtained from WT VSG vs. KO VSG mouse livers. Phosphatidylcholine (PC) was decreased in KO VSG comparing to WT VSG, while phosphatidylinositol (PI), diacylglycerol (DAG), phosphatidylglycerol (PG), and sphingomyelin (SM) were increased in KO VSG mice; *n*: WT VSG = 5, KO VSG = 5. *I*: volcano plot of 418 identified lipid compounds; 24 lipid compound ions were significantly different between WT VSG and KO VSG groups with fold change >2 and $P < 0.05$; *n*: WT VSG = 5, KO VSG = 5. *J*: principal component analysis (PCA) of mouse liver separates; 418 identified lipid compounds were analyzed in electrospray positive and negative modes from liver tissue of mice collected at 49 days postsurgery; *n*: WT VSG = 5, KO VSG = 5.

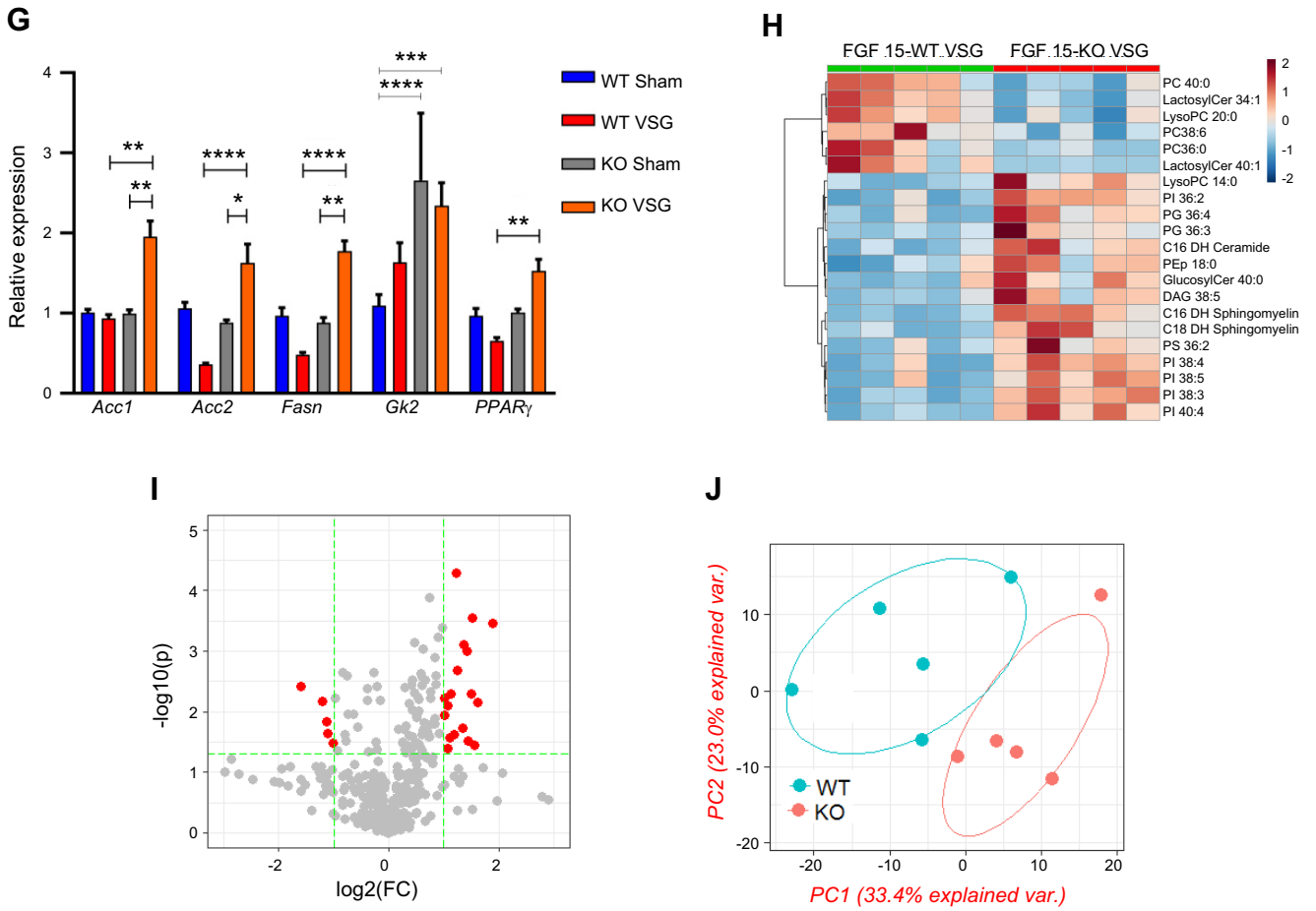

Fig. 4. —*Continued*

wherein the obesity-related ER stress phenotype is restricted to the liver in Fgf15-KO mice.

It has been recently shown that AAV-driven FGF19 administration exhibits a protective effect on intestinal epithelial barrier integrity, inhibits inflammatory immune response, and modulates gut microbial composition by induction of a beneficial bacterial shift while reducing bile acid synthesis and pool size (15). This may help explain our observation of exacerbated hepatic inflammation in mice lacking Fgf15 after VSG. Consequently, one may speculate that Fgf15 deficiency in a VSG model may contribute toward an unfavorable shift of bacterial taxa in the gut, which would result in undesired metabolic phenotypes. For instance, tenericutes, anaeroplasma, and mollicutes were all stimulated by FGF19 administration (15). While it is known that the proportion of tenericutes is significantly reduced in a mouse model of obesity and NAFLD (42), patients with hypercholesterolemia have lower abundance of anaeroplasma and mollicutes (17). However, the mechanistic role of microbiota in the benefits of bariatric surgery remains elusive, and microbial composition was not assessed in our study, thus will necessitate further investigation.

A study by McGavigan et al. (37) focused on the FXR-independent bile acid receptor Takeda G protein-coupled *receptor* 5 (*TGR5*) after VSG in mice. Located primarily in endocrine glands, adipocytes, and muscles, this receptor was found to be important for glucose tolerance improvement after VSG. Another study also suggested that TGR5 is required to mediate antiobesity, antihyperglycemia, and fatty liver improvement effects of VSG (12). The recently discovered gut-restricted TGR5 agonist bile acid CA7S has been shown to improve glucose tolerance by increasing glucagon-like peptide-1 expression and secretion (7). The role of bile acids as signaling molecules is well acknowledged, and available evidence suggests that they act through both FXR and TGR5 receptors to achieve the beneficial metabolic effects after VSG. Both receptors are viewed as targets for the development of treatment of metabolic diseases (9). We observed increased ileal bile acid levels in Fgf15-KO Sham mice (Fig. 3*E*) that may lead to increased TGR5 signaling in the colon. Future experiments with intestine-specific Fgf15 knockout mice and TGR5 knockout mice will be important to understand this key observation.

Another limitation of our study was that the experiments were performed in a total body Fgf15-KO mouse model; thus, we could not distinguish which location of Fgf15 expression was responsible for each specific effect that was observed in this study. Our previous data suggest that FGF19 acts through the brain to reduce food intake and body weight and improve glucose tolerance (46). However, to answer the questions on the level of integrated physiology and clarify signaling pathways, studies utilizing organ-specific KO mice (i.e., brain, small intestine) will need to be performed. Similarly, due to some physiological differences between murine Fgf15 and human FGF19,

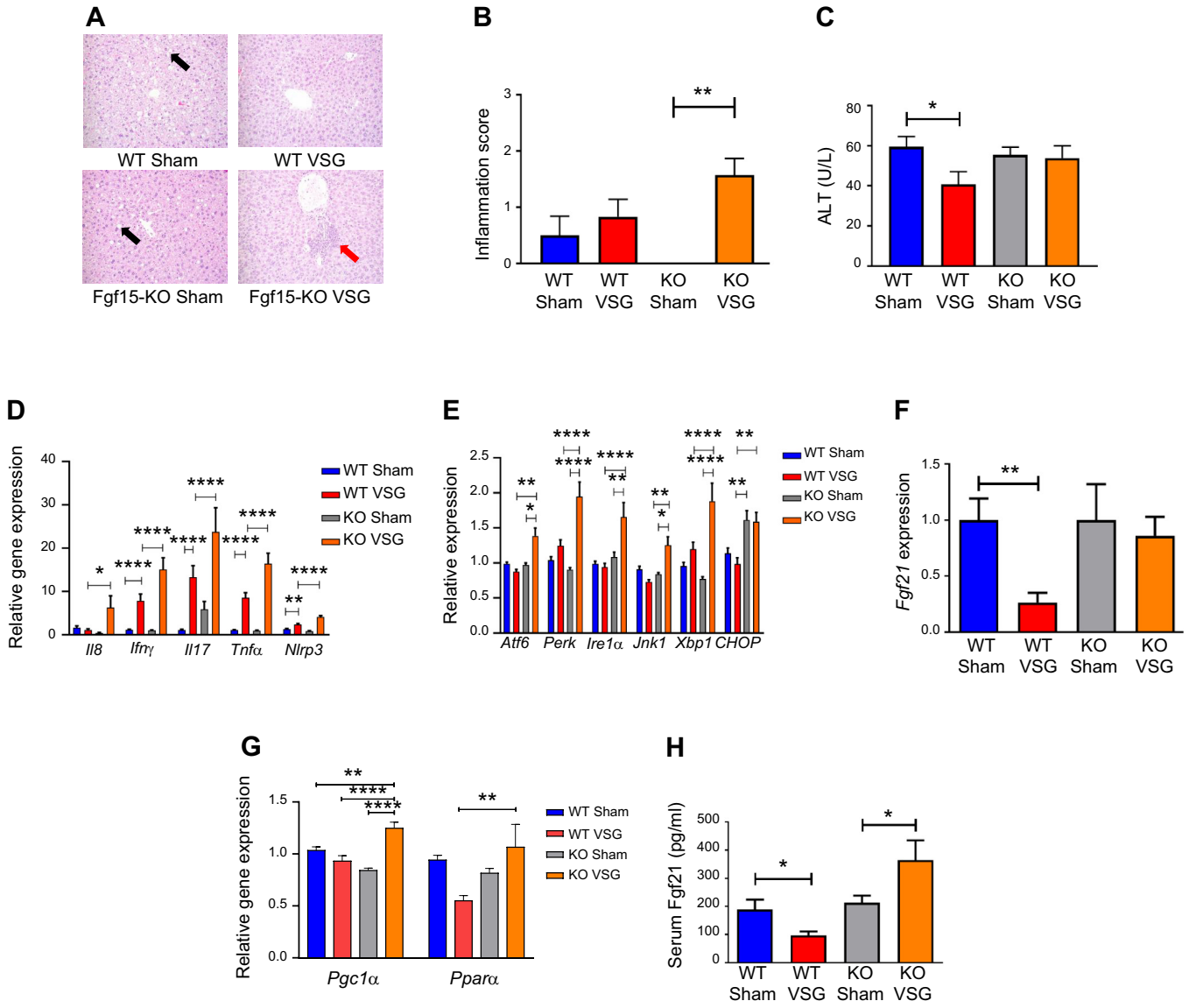

Fig. 5. Fibroblast growth factor 15 (*Fgf15*) deficiency results in increased hepatic inflammation via an endoplasmic reticulum (ER) stress mechanism post-post-vertical sleeve gastrectomy (VSG). *A*: hepatic histology 49 days postsurgery. Representative ×20 magnified hematoxylin-eosin sections showed lipid droplet accumulation in livers of Sham-operated groups (black arrow), whereas this was not observed in VSG groups. In knockout (KO) VSG mice, we observed inflammation foci in liver parenchyma (red arrow). *B*: Hepatic inflammation score 49 days postsurgery. KO VSG mice developed inflammation in liver compared with their control group, which is expressed quantitatively by inflammation score bar graph. No inflammation was observed in KO Sham liver sections; therefore, no inflammation score was plotted for same; *n*: wild-type (WT) Sham = 6, WT VSG = 6, KO Sham = 5, KO VSG = 7. $^{**}P < 0.01$, one-way ANOVA. *C*: serum alanine aminotransferase (ALT) levels 49 days postsurgery. ALT was lower in WT VSG mice compared with WT Sham mice 49 days postsurgery; *n*: WT Sham = 6, WT VSG = 6, KO Sham = 5, KO VSG = 7. $^{*}P < 0.05$, *t* test. *D*: hepatic inflammation gene expression at *day 49* postsurgery. mRNA levels of genes coding for inflammation were measured by Biomark HD System high-throughput PCR and expressed in relative expression units. Interleukin-8 (*Il8*), interferon-γ (*IFNγ*), interleukin-17 (*Il17*), tumor necrosis factor-α (*TNFα*), and *Nlrp3* (NOD-, LRR- and pyrin domain-containing protein-3) were significantly overexpressed only in KO VSG mice; *n*: WT Sham = 4, WT VSG = 5, KO Sham = 4, KO VSG = 6; $^{*}P < 0.05$, $^{**}P < 0.01$, $^{****}P < 0.0001$, one-way ANOVA, *t* test; *n*: WT Sham = 6, WT VSG = 6, KO Sham = 5, KO VSG = 7; ($^{*}P < 0.05$, $^{**}P < 0.01$, $^{****}P < 0.0001$, one-way ANOVA. *E*: hepatic ER stress gene expression at *day 49* postsurgery. mRNA levels of genes coding for ER stress were measured by Biomark HD System high-throughput PCR and expressed in relative expression units. *Atf6, Perk, Ire1a, Jnk1*, and *Xbp1* were significantly overexpressed only in KO VSG mice; *n*: WT Sham = 4, WT VSG = 5, KO Sham = 4, KO VSG = 6; $^{*}P < 0.05$, $^{**}P < 0.01$, $^{****}P < 0.0001$, one-way ANOVA, *t* test; *n*: WT Sham = 6, WT VSG = 6, KO Sham = 5, KO VSG = 7; $^{*}P < 0.05$, $^{**}P < 0.01$, $^{****}P < 0.0001$, one-way ANOVA. *F*: hepatic *Fgf21* gene expression at *day 49* postsurgery. mRNA levels of the gene coding for *Fgf21* was measured by RT-PCR and expressed in relative expression units. Fgf21 was suppressed in WT VSG compared with WT Sham group, whereas this was not observed in KO VSG mice; *n*: WT Sham = 4, WT VSG = 5, KO Sham = 4, KO VSG = 6. $^{**}P < 0.01$, one-way ANOVA, *t* test. *G*: hepatic *PPARα* (peroxisome proliferator-activated receptor-α) and *PGC-1α* (PPARγ coactivator 1α) gene expression at *day 49* postsurgery. mRNA levels of *PPAR.α* and *PGC-1α* genes were measured by Biomark HD System high-throughput PCR and expressed in relative expression units. PPARα was suppressed in WT VSG compared with KO VSG group, whereas PGC-1α was overexpressed in KO VSG mice relative to all other groups; *n*: WT Sham = 6, WT VSG = 6, KO Sham = 5, KO VSG = 7. $^{*}P < 0.05$, $^{**}P < 0.01$, $^{****}P < 0.0001$, one-way ANOVA. *H*: serum Fgf21 levels at *day 49* postsurgery. Serum Fgf21 levels were decreased in WT VSG mice, whereas they were drastically increased in KO VSG mice compared with their respective Sham controls; *n*: WT Sham = 6, WT VSG = 6, KO Sham = 5, KO VSG = 7. $^{*}P < 0.05$, one-way ANOVA, *t* test.

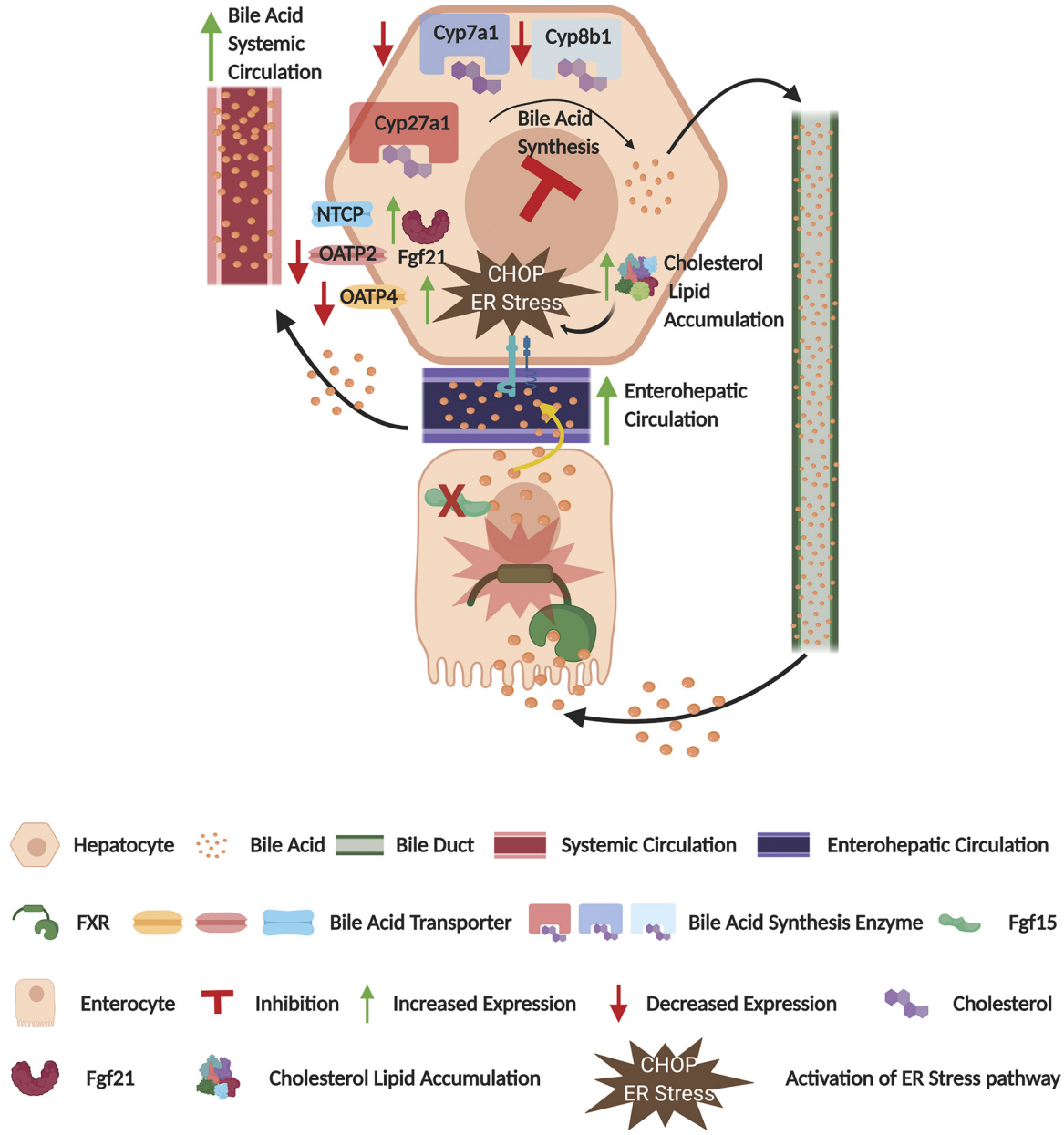

Fig. 6. Fibroblast growth factor 15 (*Fgf15*) deficiency induces cholesterol and lipid accumulation. Graphic representation of the effect of vertical sleeve gastrectomy (VSG) in *Fgf15*-deficient mice. CHOP, CCAAT enhancer-binding protein homologous protein; Cyp, cytochrome *P*-450; ER, endoplasmic reticulum; NTCP, Na^+-taurocholate-cotransporting polypeptide; OATP, organic anion transporter polypeptide.

clinical studies are needed to better understand the bile acid-FXR-FGF19 pathway's impact on metabolism and hepatic protection in obese patients that underwent VSG.

Weight loss surgery like VSG has become the best therapy for obesity and its comorbidities, including type 2 diabetes and nonalcoholic steatohepatitis (2). Our data described that, in the absence of Fgf15, VSG surgery in obese mice leads to weight loss but an incomplete commensurate improvement in glucose and liver metabolic outcomes. Second, our data introduce a potential point of distinction between bile acids acting as ligands compared with their canonical downstream signaling pathways. In conclusion, we believe that, despite these data, there still exists a lack of complete understanding bywhich specific signaling pathways bariatric surgery, such as VSG, influences glucose and lipid metabolism and thus further detailed investigations are warranted.

ACKNOWLEDGMENTS

We thank Dr. Steven Kliewer, UT Southwestern, for providing *Fgf15* knockout mice and Dr. Paul Dawson, Emory University, for supplying Fgf15 antibody.

GRANTS

This work was supported by National Institute of Diabetes and Digestive and Kidney Diseases grants awarded to D. Sandoval (R01 DK-107282), R. Kohli (R01 DK-100314), and an Ethicon Endo-Surgery grant awarded to R. Kohli.

DISCLOSURES

R.J.S. has received research support from Novo Nordisk, Zafgen, MedImmune, and Sanofi and has served as a paid consultant to Ethicon Endo-Surgery/Johnson & Johnson, Orexigen, Novo Nordisk, Daiichi Sankyo, Janssen/Johnson & Johnson, Novartis, Paul Hastings Law Firm, Scohia, and Kallyope Inc. D.A.S. receives research support from Novo Nordisk, Ethicon Endo-Surgery, and Zafgen. R.K. receives research support from Johnson & Johnson. None of the other authors has any conflicts of interest, financial or otherwise, to disclose.

AUTHOR CONTRIBUTIONS

A.M., K.D.S., R.J.S., D.A.S., R.K., J.B., and K.K.R. conceived and designed research; A.M., M.O., D.A.S., R.K., J.B., R.S., B.T., S.M., D.F., W.Z. and X.Z. performed experiments; A.M., K.D.S., R.J.S., D.A.S., R.K., J.B., R.S., and K.K.R. analyzed data; A.M., D.A.S., R.K., J.B., W.Z. and X.Z. interpreted results of experiments; A.M. and J.B. prepared figures; A.M. and J.B. drafted manuscript; A.M., M.O., K.D.S., R.J.S., D.A.S., R.K., J.B., R.S., B.T., S.M., D.F., K.K.R., W.Z. and X.Z. edited and revised manuscript; A.M., M.O., K.D.S., R.J.S., D.A.S., R.K., J.B., R.S., B.T., S.M., D.F., K.K.R., W.Z. and X.Z. approved final version of manuscript.

REFERENCES

1. **Al-Khaifi A**, **Rudling M**, **Angelin B.** An FXR agonist reduces bile acid synthesis independently of increases in FGF19 in healthy volunteers. *Gastroenterology* 155: 1012–1016, 2018. doi:10.1053/j.gastro.2018.06.038.
2. **Angrisani L**, **Santonicola A**, **Iovino P**, **Vitiello A**, **Zundel N**, **Buchwald H**, **Scopinaro N.** Bariatric surgery and endoluminal procedures: IFSO worldwide survey 2014. *Obes Surg* 27: 2279–2289, 2017 [Erratum *Obes Surg* 27: 2290–2292, 2017]. doi:10.1007/s11695-017-2666-x.
3. **Asrih M**, **Montessuit C**, **Philippe J**, **Jornayvaz FR.** Free fatty acids impair FGF21 action in HepG2 cells. *Cell Physiol Biochem* 37: 1767–1778, 2015. doi:10.1159/000438540.
4. **Camporez JP**, **Kanda S**, **Petersen MC**, **Jornayvaz FR**, **Samuel VT**, **Bhanot S**, **Petersen KF**, **Jurczak MJ**, **Shulman GI.** ApoA5 knockdown improves whole-body insulin sensitivity in high-fat-fed mice by reducing ectopic lipid content. *J Lipid Res* 56: 526–536, 2015. doi:10.1194/jlr.M054080.
5. **Cariou B**, **van Harmelen K**, **Duran-Sandoval D**, **van Dijk TH**, **Grefhorst A**, **Abdelkarim M**, **Caron S**, **Torpier G**, **Fruchart JC**, **Gonzalez FJ**, **Kuipers F**, **Staels B.** The farnesoid X receptor modulates adiposity and peripheral insulin sensitivity in mice. *J Biol Chem* 281: 11039–11049, 2006. doi:10.1074/jbc.M510258200.
6. **Carter JR**, **Kennedy EP.** Enzymatic synthesis of cytidine diphosphate diglyceride. *J Lipid Res* 7: 678–683, 1966.
7. **Chaudhari SN**, **Harris DA**, **Aliakbarian H**, **Luo JN**, **Henke MT**, **Subramaniam R**, **Vernon AH**, **Tavakkoli A**, **Sheu EG**, **Devlin AS.** Bariatric surgery reveals a gut-restricted TGR5 agonist with anti-diabetic effects. *Nat Chem Biol*, In press. doi:10.1038/s41589-020-0604-z.
8. **Chiang JY.** Bile acid metabolism and signaling. *Compr Physiol* 3: 1191–1212, 2013. doi:10.1002/cphy.c120023.
9. **Chiang JYL**, **Ferrell JM.** Bile acid receptors FXR and TGR5 signaling in fatty liver diseases and therapy. *Am J Physiol Gastrointest Liver Physiol* 318: G554–G573, 2020. doi:10.1152/ajpgi.00223.2019.
10. **Cho H**, **Mu J**, **Kim JK**, **Thorvaldsen JL**, **Chu Q**, **Crenshaw EB III**, **Kaestner KH**, **Bartolomei MS**, **Shulman GI**, **Birnbaum MJ.** Insulin resistance and a diabetes mellitus-like syndrome in mice lacking the protein kinase Akt2 (PKB beta). *Science* 292: 1728–1731, 2001. doi:10.1126/science.292.5522.1728.
11. **Afshin A**, **Forouzanfar MH**, **Reitsma MB**, **Sur P**, **Estep K**, **Lee A**, **Marczak L**, **Mokdad AH**, **Moradi-Lakeh M**, **Naghavi M**; **GBD 2015 Obesity Collaborators.** Health Effects of Overweight and Obesity in 195 Countries over 25 Years. *N Engl J Med* 377: 13–27, 2017. doi:10.1056/NEJMoa1614362.
12. **Ding L**, **Sousa KM**, **Jin L**, **Dong B**, **Kim BW**, **Ramirez R**, **Xiao Z**, **Gu Y**, **Yang Q**, **Wang J**, **Yu D**, **Pigazzi A**, **Schones D**, **Yang L**, **Moore D**, **Wang Z**, **Huang W.** Vertical sleeve gastrectomy activates GPBAR-1/TGR5 to sustain weight loss, improve fatty liver, and remit insulin resistance in mice. *Hepatology* 64: 760–773, 2016. doi:10.1002/hep.28689.
13. **Emanuelli B**, **Vienberg SG**, **Smyth G**, **Cheng C**, **Stanford KI**, **Arumugam M**, **Michael MD**, **Adams AC**, **Kharitonenkov A**, **Kahn CR.** Interplay between FGF21 and insulin action in the liver regulates metabolism. *J Clin Invest* 124: 515–527, 2014. doi:10.1172/JCI67353.
14. **Funke A**, **Schreurs M**, **Aparicio-Vergara M**, **Sheedfar F**, **Gruben N**, **Kloosterhuis NJ**, **Shiri-Sverdlov R**, **Groen AK**, **van de Sluis B**, **Hofker MH**, **Koonen DP.** Cholesterol-induced hepatic inflammation does not contribute to the development of insulin resistance in male LDL receptor knockout mice. *Atherosclerosis* 232: 390–396, 2014. doi:10.1016/j.atherosclerosis.2013.11.074.
15. **Gadaleta RM**, **Garcia-Irigoyen O**, **Cariello M**, **Scialpi N**, **Peres C**, **Vetrano S**, **Fiorino G**, **Danese S**, **Ko B**, **Luo J**, **Porru E**, **Roda A**, **Sabbà C**, **Moschetta A.** Fibroblast Growth Factor 19 modulates intestinal microbiota and inflammation in presence of Farnesoid X Receptor. *EBioMedicine* 54: 102719, 2020 [Erratum in *EBioMedicine* 57: 102873, 2020]. doi:10.1016/j.ebiom.2020.102719.
16. **Grabon A**, **Bankaitis VA**, **McDermott MI.** The interface between phosphatidylinositol transfer protein function and phosphoinositide signaling in higher eukaryotes. *J Lipid Res* 60: 242–268, 2019. doi:10.1194/jlr.R089730.
17. **Granado-Serrano AB**, **Martín-Garí M**, **Sánchez V**, **Riart Solans M**, **Berdún R**, **Ludwig IA**, **Rubió L**, **Vilaprinyó E**, **Portero-Otín M**, **Serrano JCE.** Faecal bacterial and short-chain fatty acids signature in hypercholesterolemia. *Sci Rep* 9: 1772, 2019. doi:10.1038/s41598-019-38874-3.
18. **Hagio M**, **Matsumoto M**, **Fukushima M**, **Hara H**, **Ishizuka S.** Improved analysis of bile acids in tissues and intestinal contents of rats using LC/ESI-MS. *J Lipid Res* 50: 173–180, 2009. doi:10.1194/jlr.D800041-JLR200.
19. **Haluzíková D**, **Lacinová Z**, **Kaválková P**, **Drápalová J**, **Krõízõová J**, **Bártlová M**, **Mráz M**, **Petr T**, **Vítek L**, **Kasalický M**, **Haluzík M.** Laparoscopic sleeve gastrectomy differentially affects serum concentrations of FGF-19 and FGF-21 in morbidly obese subjects. *Obesity (Silver Spring)* 21: 1335–1342, 2013. doi:10.1002/oby.20208.
20. **Hansen AMK**, **Vienberg SG**, **Lykkegaard K**, **Zhao X**, **Tingqing G**, **Han D**, **Zhang X**, **Thøgersen H**, **Sass-Ørum K**, **Tagmose T**, **Raun K**, **Andersen B.** Differential receptor selectivity of the FGF15/FGF19 orthologues determines distinct metabolic activities in *db*/*db* mice. *Biochem J* 475: 2985–2996, 2018. doi:10.1042/BCJ20180555.
21. **Hay N.** Akt isoforms and glucose homeostasis - the leptin connection. *Trends Endocrinol Metab* 22: 66–73, 2011. doi:10.1016/j.tem.2010.09.003.
22. **Inagaki T**, **Choi M**, **Moschetta A**, **Peng L**, **Cummins CL**, **McDonald JG**, **Luo G**, **Jones SA**, **Goodwin B**, **Richardson JA**, **Gerard RD**, **Repa JJ**, **Mangelsdorf DJ**, **Kliewer SA.** Fibroblast growth factor 15 functions as an enterohepatic signal to regulate bile acid homeostasis. *Cell Metab* 2: 217–225, 2005. doi:10.1016/j.cmet.2005.09.001.
23. **Jakicic JM**, **King WC**, **Marcus MD**, **Davis KK**, **Helsel D**, **Rickman AD**, **Gibbs BB**, **Rogers RJ**, **Wahed A**, **Belle SH.** Short-term weight loss with diet and physical activity in young adults: the IDEA study. *Obesity (Silver Spring)* 23: 2385–2397, 2015. doi:10.1002/oby.21241.
24. **Jiang C**, **Xie C**, **Li F**, **Zhang L**, **Nichols RG**, **Krausz KW**, **Cai J**, **Qi Y**, **Fang ZZ**, **Takahashi S**, **Tanaka N**, **Desai D**, **Amin SG**, **Albert I**, **Patterson AD**, **Gonzalez FJ.** Intestinal farnesoid X receptor signaling promotes nonalcoholic fatty liver disease. *J Clin Invest* 125: 386–402, 2015. doi:10.1172/JCI76738.
25. **Jiang S**, **Yan C**, **Fang QC**, **Shao ML**, **Zhang YL**, **Liu Y**, **Deng YP**, **Shan B**, **Liu JQ**, **Li HT**, **Yang L**, **Zhou J**, **Dai Z**, **Liu Y**, **Jia WP.** Fibroblast growth factor 21 is regulated by the IRE1α-XBP1 branch of the unfolded protein response and counteracts endoplasmic reticulum stress-induced hepatic steatosis. *J Biol Chem* 289: 29751–29765, 2014. doi:10.1074/jbc.M114.565960.
26. **Joe Y**, **Kim S**, **Kim HJ**, **Park J**, **Chen Y**, **Park HJ**, **Jekal SJ**, **Ryter SW**, **Kim UH**, **Chung HT.** FGF21 induced by carbon monoxide mediates metabolic homeostasis via the PERK/ATF4 pathway. *FASEB J* 32: 2630–2643, 2018. doi:10.1096/fj.201700709RR.
27. **Kindel TL**, **Krause C**, **Helm MC**, **McBride CL**, **Oleynikov D**, **Thakare R**, **Alamoudi J**, **Kothari V**, **Alnouti Y**, **Kohli R.** Increased glycine-amidated hyocholic acid correlates to improved early weight loss after sleeve gastrectomy. *Surg Endosc* 32: 805–812, 2018. doi:10.1007/s00464-017-5747-y.
28. **Kir S**, **Beddow SA**, **Samuel VT**, **Miller P**, **Previs SF**, **Suino-Powell K**, **Xu HE**, **Shulman GI**, **Kliewer SA**, **Mangelsdorf DJ.** FGF19 as a postprandial, insulin-independent activator of hepatic protein and glycogen synthesis. *Science* 331: 1621–1624, 2011. doi:10.1126/science.1198363.
29. **Kohli R**, **Kirby M**, **Setchell KD**, **Jha P**, **Klustaitis K**, **Woollett LA**, **Pfluger PT**, **Balistreri WF**, **Tso P**, **Jandacek RJ**, **Woods SC**, **Heubi JE**, **Tschoep MH**, **D'Alessio DA**, **Shroyer NF**, **Seeley RJ.** Intestinal adaptation after ileal interposition surgery increases bile acid recycling and protects

against obesity-related comorbidities. *Am J Physiol Gastrointest Liver Physiol* 299: G652–G660, 2010. doi:10.1152/ajpgi.00221.2010.

30. **Kong B**, **Huang J**, **Zhu Y**, **Li G**, **Williams J**, **Shen S**, **Aleksunes LM**, **Richardson JR**, **Apte U**, **Rudnick DA**, **Guo GL.** Fibroblast growth factor 15 deficiency impairs liver regeneration in mice. *Am J Physiol Gastrointest Liver Physiol* 306: G893–G902, 2014. doi:10.1152/ajpgi.00337.2013.
31. **Kumashiro N**, **Erion DM**, **Zhang D**, **Kahn M**, **Beddow SA**, **Chu X**, **Still CD**, **Gerhard GS**, **Han X**, **Dziura J**, **Petersen KF**, **Samuel VT**, **Shulman GI.** Cellular mechanism of insulin resistance in nonalcoholic fatty liver disease. *Proc Natl Acad Sci USA* 108: 16381–16385, 2011. doi:10.1073/pnas.1113359108.
32. **Kwon J**, **Kim B**, **Lee C**, **Joung H**, **Kim BK**, **Choi IS**, **Hyun CK.** Comprehensive amelioration of high-fat diet-induced metabolic dysfunctions through activation of the PGC-1α pathway by probiotics treatment in mice. *PLoS One* 15: e0228932, 2020. doi:10.1371/journal.pone.0228932.
33. **Kyrou I**, **Randeva HS**, **Tsigos C**, **Kaltsas G**, **Weickert MO.** Clinical problems caused by obesity. In: *Endotext*, edited by Feingold KR, Anawalt B, Boyce A, Chrousos G, de Herder WW, Dungan K, Grossman A, Hershman JM, Hofland HJ, Kaltsas G, Koch C, Kopp P, Korbonits M, McLachlan R, Morley JE, New M, Purnell J, Singer F, Stratakis CA, Trence DL, Wilson DP. South Dartmouth, MA: MDText.com, Inc. 2000.
34. **Lee JM**, **Ong JR**, **Vergnes L**, **de Aguiar Vallim TQ**, **Nolan J**, **Cantor RM**, **Walters JRF**, **Reue K.** Diet1, bile acid diarrhea, and FGF15/19: mouse model and human genetic variants. *J Lipid Res* 59: 429–438, 2018. doi:10.1194/jlr.M078279.
35. **Lundåsen T**, **Hunt MC**, **Nilsson LM**, **Sanyal S**, **Angelin B**, **Alexson SE**, **Rudling M.** PPARalpha is a key regulator of hepatic FGF21. *Biochem Biophys Res Commun* 360: 437–440, 2007. doi:10.1016/j.bbrc.2007.06.068.
36. **Mahe MM**, **Aihara E**, **Schumacher MA**, **Zavros Y**, **Montrose MH**, **Helmrath MA**, **Sato T**, **Shroyer NF.** Establishment of gastrointestinal epithelial organoids. *Curr Protoc Mouse Biol* 3: 217–240, 2013. doi:10.1002/9780470942390.mo130179.
37. **McGavigan AK**, **Garibay D**, **Henseler ZM**, **Chen J**, **Bettaieb A**, **Haj FG**, **Ley RE**, **Chouinard ML**, **Cummings BP.** TGR5 contributes to glucoregulatory improvements after vertical sleeve gastrectomy in mice. *Gut* 66: 226–234, 2017. doi:10.1136/gutjnl-2015-309871.
38. **Mutanen A**, **Lohi J**, **Heikkilä P**, **Jalanko H**, **Pakarinen MP.** Loss of ileum decreases serum fibroblast growth factor 19 in relation to liver inflammation and fibrosis in pediatric onset intestinal failure. *J Hepatol* 62: 1391–1397, 2015. doi:10.1016/j.jhep.2015.01.004.
39. **Myronovych A**, **Kirby M**, **Ryan KK**, **Zhang W**, **Jha P**, **Setchell KD**, **Dexheimer PJ**, **Aronow B**, **Seeley RJ**, **Kohli R.** Vertical sleeve gastrectomy reduces hepatic steatosis while increasing serum bile acids in a weight-loss-independent manner. *Obesity (Silver Spring)* 22: 390–400, 2014. doi:10.1002/oby.20548.
40. **Myronovych A**, **Salazar-Gonzalez RM**, **Ryan KK**, **Miles L**, **Zhang W**, **Jha P**, **Wang L**, **Setchell KD**, **Seeley RJ**, **Kohli R.** The role of small heterodimer partner in nonalcoholic fatty liver disease improvement after sleeve gastrectomy in mice. *Obesity (Silver Spring)* 22: 2301–2311, 2014. doi:10.1002/oby.20890.
41. **Negroni A**, **Fiaschini N**, **Palone F**, **Vitali R**, **Colantoni E**, **Laudadio I**, **Oliva S**, **Aloi M**, **Cucchiara S**, **Stronati L.** Intestinal inflammation alters the expression of hepatic bile acid receptors causing liver impairment. *J Pediatr Gastroenterol Nutr* 71: 189–196, 2020. doi:10.1097/MPG.0000000000002759.
42. **Porras D**, **Nistal E**, **Martínez-Flórez S**, **González-Gallego J**, **García-Mediavilla MV**, **Sánchez-Campos S.** Intestinal microbiota modulation in obesity-related non-alcoholic fatty liver disease. *Front Physiol* 9: 1813, 2018. doi:10.3389/fphys.2018.01813.
43. **Potthoff MJ**, **Kliewer SA**, **Mangelsdorf DJ.** Endocrine fibroblast growth factors 15/19 and 21: from feast to famine. *Genes Dev* 26: 312–324, 2012. doi:10.1101/gad.184788.111.
44. **Prawitt J**, **Abdelkarim M**, **Stroeve JH**, **Popescu I**, **Duez H**, **Velagapudi VR**, **Dumont J**, **Bouchaert E**, **van Dijk TH**, **Lucas A**, **Dorchies E**, **Daoudi M**, **Lestavel S**, **Gonzalez FJ**, **Oresic M**, **Cariou B**, **Kuipers F**, **Caron S**, **Staels B.** Farnesoid X receptor deficiency improves glucose homeostasis in mouse models of obesity. *Diabetes* 60: 1861–1871, 2011. doi:10.2337/db11-0030.
45. **Qi J**, **Lang W**, **Giardino E**, **Caldwell GW**, **Smith C**, **Minor LK**, **Darrow AL**, **Willemsens G**, **Dewaepenaert K**, **Roevens P**, **Linders JT**, **Liang Y**, **Connelly MA.** High-content assays for evaluating cellular and hepatic diacylglycerol acyltransferase activity. *J Lipid Res* 51: 3559–3567, 2010. doi:10.1194/jlr.D008029.
46. **Ryan KK**, **Kohli R**, **Gutierrez-Aguilar R**, **Gaitonde SG**, **Woods SC**, **Seeley RJ.** Fibroblast growth factor-19 action in the brain reduces food intake and body weight and improves glucose tolerance in male rats. *Endocrinology* 154: 9–15, 2013. doi:10.1210/en.2012-1891.
47. **Ryan KK**, **Tremaroli V**, **Clemmensen C**, **Kovatcheva-Datchary P**, **Myronovych A**, **Karns R**, **Wilson-Pérez HE**, **Sandoval DA**, **Kohli R**, **Bäckhed F**, **Seeley RJ.** FXR is a molecular target for the effects of vertical sleeve gastrectomy. *Nature* 509: 183–188, 2014. doi:10.1038/nature13135.
48. **Sachdev S**, **Wang Q**, **Billington C**, **Connett J**, **Ahmed L**, **Inabnet W**, **Chua S**, **Ikramuddin S**, **Korner J.** FGF 19 and bile acids increase following Roux-en-Y gastric bypass but not after medical management in patients with type 2 diabetes. *Obes Surg* 26: 957–965, 2016. doi:10.1007/s11695-015-1834-0.
49. **Samuel VT**, **Liu ZX**, **Wang A**, **Beddow SA**, **Geisler JG**, **Kahn M**, **Zhang XM**, **Monia BP**, **Bhanot S**, **Shulman GI.** Inhibition of protein kinase Cepsilon prevents hepatic insulin resistance in nonalcoholic fatty liver disease. *J Clin Invest* 117: 739–745, 2007. doi:10.1172/JCI30400.
50. **Schaap FG**, **Kremer AE**, **Lamers WH**, **Jansen PL**, **Gaemers IC.** Fibroblast growth factor 21 is induced by endoplasmic reticulum stress. *Biochimie* 95: 692–699, 2013. doi:10.1016/j.biochi.2012.10.019.
51. **Schumacher JD**, **Kong B**, **Pan Y**, **Zhan L**, **Sun R**, **Aa J**, **Rizzolo D**, **Richardson JR**, **Chen A**, **Goedken M**, **Aleksunes LM**, **Laskin DL**, **Guo GL.** The effect of fibroblast growth factor 15 deficiency on the development of high fat diet induced non-alcoholic steatohepatitis. *Toxicol Appl Pharmacol* 330: 1–8, 2017. doi:10.1016/j.taap.2017.06.023.
52. **Seeley RJ**, **Chambers AP**, **Sandoval DA.** The role of gut adaptation in the potent effects of multiple bariatric surgeries on obesity and diabetes. *Cell Metab* 21: 369–378, 2015. doi:10.1016/j.cmet.2015.01.001.
53. **Simon JB**, **Scheig R.** Serum cholesterol esterification in liver disease. *N Engl J Med* 283: 841–846, 1970. doi:10.1056/NEJM197010152831604.
54. **Taniguchi CM**, **Tran TT**, **Kondo T**, **Luo J**, **Ueki K**, **Cantley LC**, **Kahn CR.** Phosphoinositide 3-kinase regulatory subunit p85alpha suppresses insulin action via positive regulation of PTEN. *Proc Natl Acad Sci USA* 103: 12093–12097, 2006 [Erratum in *Proc Natl Acad Sci USA* 113: E3588, 2016]. doi:10.1073/pnas.0604628103.
55. **Wishart DS**, **Feunang YD**, **Marcu A**, **Guo AC**, **Liang K**, **Vázquez-Fresno R**, **Sajed T**, **Johnson D**, **Li C**, **Karu N**, **Sayeeda Z**, **Lo E**, **Assempour N**, **Berjanskii M**, **Singhal S**, **Arndt D**, **Liang Y**, **Badran H**, **Grant J**, **Serra-Cayuela A**, **Liu Y**, **Mandal R**, **Neveu V**, **Pon A**, **Knox C**, **Wilson M**, **Manach C**, **Scalbert A.** HMDB 4.0: the human metabolome database for 2018. *Nucleic Acids Res* 46: D608–D617, 2018. doi:10.1093/nar/gkx1089.
56. **Wolfe BM**, **Kvach E**, **Eckel RH.** Treatment of obesity: weight loss and bariatric surgery. *Circ Res* 118: 1844–1855, 2016. doi:10.1161/CIRCRESAHA.116.307591.
57. **Yvan-Charvet L**, **Ranalletta M**, **Wang N**, **Han S**, **Terasaka N**, **Li R**, **Welch C**, **Tall AR.** Combined deficiency of ABCA1 and ABCG1 promotes foam cell accumulation and accelerates atherosclerosis in mice. *J Clin Invest* 117: 3900–3908, 2007. doi:10.1172/JCI33372.
58. **Zhao X**, **Brusadelli MG**, **Sauter S**, **Butsch Kovacic M**, **Zhang W**, **Romick-Rosendale LE**, **Lambert PF**, **Setchell KDR**, **Wells SI.** Lipidomic profiling links the Fanconi anemia pathway to glycosphingolipid metabolism in head and neck cancer cells. *Clin Cancer Res* 24: 2700–2709, 2018. doi:10.1158/1078-0432.CCR-17-3686.
59. **Zhou M**, **Luo J**, **Chen M**, **Yang H**, **Learned RM**, **DePaoli AM**, **Tian H**, **Ling L.** Mouse species-specific control of hepatocarcinogenesis and metabolism by FGF19/FGF15. *J Hepatol* 66: 1182–1192, 2017. doi:10.1016/j.jhep.2017.01.027.